UNIVERSITÀ DEGLI STUDI DI NAPOLI
FEDERICO II

International Phd Program On:

Novel Technologies for Materials, Sensors and Imaging

XXVII cycle

FROM GRAPHENE TO GRAPHENE-BASED GAS SENSORS OPERATING IN ENVIRONMENTAL CONDITIONS

FILIBERTO RICCIARDELLA

Supervisor
Dr. Tiziana Polichetti

Academic tutor
Prof. Domenico Ninno

"Populus me sibilat, at mihi plaudo
Ipse domi simul ac nummos contemplar in arca"
(Orazio, Satire, 1, 1, 66-67)

To my tutor Tiziana

SUMMARY

CHAPTER I

INTRODUCTION

1.1 General notes on pollution Pag 5
1.2 Dangerous analytes and limits of exposure ″ 7
1.3 The role of the nanotechnology ″ 9
1.4 Goals and outline of the thesis ″ 11

CHAPTER II

ROUTES FOR GRAPHENE PREPARATION

2.1 The graphene preparation methods: an overview Pag 13
2.1.1 Chemical Vapor Deposition ″ 17
2.1.2 Thermal decomposition of silicon carbide ″ 20
2.1.3 Mechanical cleavage ″ 22
2.1.4 Electrochemical methods ″ 23
2.1.5 Laser ablation ″ 25
2.1.6 Liquid Phase Exfoliation of Graphite Oxide ″ 26
2.1.7 Liquid Phase Exfoliation of Graphite ″ 27
2.2 A challenge for sensing ″ 29

CHAPTER III

MATERIAL PREPARATION AND CHARACTERIZATION

3.1 Liquid Phase Exfoliation: the procedure Pag 32
3.2 Characterization of LPE graphene ″ 34
3.2.1 Transmission Electron and Atomic Force Microscopy characterizations ″ 41
3.3 Chemical Vapor Deposition: the procedure ″ 44
3.4 Characterization of CVD graphene ″ 48
3.5 Conclusions ″ 52

CHAPTER IV

GRAPHENE-BASED CHEMIRESISTORS FOR NO_2 DETECTION

4.1	Notes on devices preparation and experimental set up	Pag 53
	4.1.1 Differences from device-to-device performances	″ 56
	4.1.2 A simple method to recover the graphene-based chemi-resistor signal	″ 60
4.2	A new approach for the sensor response	″ 63
4.3	Sensor calibration	″ 67
4.4	Preliminary results towards other analytes	″ 71
4.5	Chemi-resistor based on CVD grown graphene	″ 74
4.6	Conclusions	″ 80

APPENDICES

A	Alumina transducer details	Pag 82
B	Gas Sensor Characterization System	″ 83
C	Abbreviations and acronyms	″ 85

CONCLUSIONS ″ 87

SCIENTIFIC PRODUCTION ″ 90

REFERENCES ″ 92

ACKNOWLEDGEMENTS ″ 102

CHAPTER I
INTRODUCTION

This Chapter represents an introduction to the present Thesis, entirely carried out at the ENEA Research Centre in Portici (Naples) - Laboratory for Materials and Devices Basic Research.

In the present section, after some generalities regarding the pollution and its possible damages, I provide a quick look on the dangerous analytes which the graphene-based gas sensors would be sensible to. Notes on limits of exposure related to these analytes are also given. In addition, an overview on the role of nano-materials and nano-technology for the detection of low concentrations is discussed, focusing in particular on graphene properties related to the sensing field. Finally, the definition of the research problems and the outline of the thesis are presented.

1.1 General notes on pollution

Emissions of pollutants almost rise from all economic, societal or domestic activities.

In the last decade, the ongoing growth of the industial production has led to the increase of the air pollution. Hand in hand, on one side, the increasing need to protect the environment has requested to detect ultra-low concentration of chemical and biological molecules; on the other side, the detection of volatile organic compounds (VOCs) or smells generated from food or household products has also become increasingly important in food industry and in indoor air quality. In fact, the quality of the human life is strictly dependent on the air quality, admitting that the network existing between these two aspects is quite widespread. To confirm this, the list below reports some of the main effects that could be caused by the air pollution:

- damages to human health as result of exposure or intake of pollutants transported through the air, deposited and accumulated in the food chain;

- acidification and eutrophication of ecosystems, with possible changes in species diversity;
- damages, yield losses affecting flora and contribution to climate forcing;
- impacts of heavy metals and persistent organic pollutants on ecosystems, due to their environmental toxicity and due to bioaccumulation;
- damages to materials and cultural heritage due to soiling and exposure to acidifying pollutants [31].

As it clearly appears, the pollution consequences cover a large spectrum of present and future human life, ranging from food contamination to monuments damages, from planet's climate to ecosystem modifications; therefore, it is straightforward, if not mandatory, that the reduction of air pollution and the improvement of air quality remain a key priority under all points of view to the aim to get better all aspects of human life.

1.2 Dangerous analytes and limits of exposure

In almost all the above mentioned effects, NH_3 (ammonia) and NO_X (nitrogen oxides) play a fundamental role.

Nitrogen oxides are emitted during fuel combustion, such as road transport, industrial facilities and, generally, high temperature combustion processes. Among the NO_X species, nitrogen dioxide (NO_2), a reactive gas mainly formed by oxidation of NO, is associated with adverse effects on health, as high concentrations cause inflammation of the airways and reduction of the lung function. NO_X also contributes to the formation of secondary inorganic PM (Particulate Matter) and O_3 (ozone) with associated effects on health and ecosystems.

NH_3 is almost entirely produced from the agricultural sector and manure management: in 2010, e.g., such sector was responsible for 94 % of the total NH_3 emissions in the EU (European Union) [31]. Also the production of fertilizer, chemicals, refrigeration systems, medical diagnosis system and material processing have a notable role in the NH_3 emissions so that its global production exceeds from 100 million tons per annum [6]. This toxic gas has been demonstrated to have significant negative impacts on health and the environment, determining disease symptoms and work-shift declines in pulmonary function or contributing in the early faint sun problem [7].

Here is, therefore, why these two kinds of analytes are among the most treated for the research in the gas sensing field. Last but not least, from a chemi – physical point of view, NO_2 and NH_3, respectively, represent the archetype of oxidant and reducing gases, so that they are frequently used in the laboratories to study and eventually predict the behavior of similar species even more aggressive than these.

However, the dangerousness towards analytes mostly depends on some parameters related to the exposure time. To this aim, different definitions of limit values and accordingly thresholds can be considered, taking into account different endpoints or averaging times.

In USA, for example, some of the recommendations sources in regards to occupational exposure limits have set the thresholds which should not be exceeded: the National Institute for Occupational Safety and Health (NIOSH) has set at 25 ppm (parts-per-milion) the time-weighted average (TWA) exposure at NH_3 for 15

min; the Occupational Safety and Health Administration (OSHA) permissible exposure limit (PEL) for NH_3 is 35 ppm as a 15 min short-term exposure limit (STEL). For NO_2, instead, a TWA has not been defined, but a “ceiling limit” at 1 ppm has been established, being the “ceiling limit" the concentration of a substance in air which may not be exceeded at any time during the work period; a STEL, instead, is basically a ceiling limit but in an averaging time of 15-min [31, 91]. By the way, in 2010, EPA (USA Environmental Protection Ambient) set a 1-hour NO_2 standard at the level of 100 parts per billion (ppb) and also retained the annual average NO_2 standard of 53 ppb [41].

In EU, instead, the Air Quality Directive 2008/50/EC set legally thresholds for ground-level concentrations of outdoor individual air pollutants that must not be exceeded. Analogously to the USA normative, limit and target values are accompanied by an averaging period, including also the number of exceedences allowed per year, if any. The parameters set by EU refer to World Health Organization (WHO) air quality guidelines (AQG), which are often more stringent than current EU target and limit values.

For example, the NO_2 limit value for the protection of human health for an averaging period of one hour is 200 $\mu g/m^3$, corresponding at about 286 ppb, and it must not be exceeded more than 18 times in a calendar year; for an averaging period of one year, instead, the limit value is 40 $\mu g/m^3$, that corresponds at about 60 ppb. Regarding to the protection of vegetation, the concentration critical levels for an averaging period of one year is about 43 ppb [31, 83]. A similar European directive for NH_3, VOCs and other atmospheric pollutants, sets the national emission ceilings limit, expressed in kilotonnes, to be not exceeded in a calendar year [84].

This brief survey wants to highlight how, independently from the various definitions and the countries taken into account, the analytes concentration ranges to not exceed are quite stringent. Indeed, the general aim of research and technology is to find routes and tools to make possible the detection and measurement of gases at levels of ppm and also lower.

1.3 The role of the nanotechnology

In the frame depicted above, the role of the nanotechnology[1] appears unbelievable indispensable. The recent development in the field of the nano-science has allowed, in fact, both to realize gas-sensors by employing several kinds of nano-materials and to achieve the issues to detect and measure more and more small amounts of a wide range of gaseous chemical compounds, also exploiting the properties of the materials at this scale.

Among the sensitive nano-materials, the most investigated class is formed by the metal oxides, typically SnO_2, TiO_2, In_2O_3, WO_3, NiO. The metal oxides sensors, often called MOX (from Metal Oxide) or semiconductor sensors, are considered the best option for the gas sensing application. In their simplest configuration, they consist of a substrate with a heater, electrodes and the sensitive layer in contact with the electrodes [17, 78, 86].

This kind of devices has been demonstrated to work perfectly at high temperatures (>350°C) and are particularly appealing as gas sensors for a series of characteristics, in parts reported in the following [87]:

- low cost, small size and easy to handle (compared to other gas sensors)
- fast sensor response and recovery[2]
- robust construction and good mechanical strength
- long operating life.

However, if the goal is to work in environmental conditions and at Room Temperature (RT), as discussed in the previous paragraph, the MOX gas sensors do not represent the best choice basically for two reasons:

1. in these scenarios their performances strongly get worse;
2. they present a high power consumption due to the working conditions at high temperature [17].

In this respect, other classes of sensitive nano-materials result to be more suitable, i.e. films based on polymers, optical fibers or organic materials and carbon nano-materials, particularly carbon nanotubes (CNTs) and graphene [9, 13]. In the

[1] The prefix "nano" refers to everything, particles, sheets, etc., that has almost one dimension ranging from 1 to 100 nanometers.

[2] These sensor's parameters will be deeply treated in the following. Briefly, the "response" is the ability of the device to react upon the gas interaction while the "recovery" is the sensor property to return at the initial conditions after the signal output.

last two decades, CNTs have become the most studied carbon nano-material for developing gas sensors operating at RT, but the rapidly rise of graphene is challenging the dominance of them [14]. The discovery of graphene in 2004, in fact, has opened unprecedented opportunity, allowing to detect and measure down to a single molecule [25, 70-71].

What is graphene and why it reveals so powerful? I will try to completely answer to the second question in this booklet, by deeply analyzing the material properties; instead, concerning the first question, the answer permits to briefly explain the potentiality of the material in the sensing field. Graphene is the name given to a two-dimensional (2D) fabric of sp^2-hybridized carbon and, most importantly, it can freely exist at RT [70, 82]. The two-dimensionality and the absence of bulk perfectly match the conditions to make graphene suitable as sensitive layer for the detection of different gases.

1. In fact, having a large theoretical specific surface area, equal to 2630 m^2g^{-1}, graphene provides the highest sensing area per unit volume so that all atoms can be considered as surface atoms and the interaction between the adsorbates and the sheet involves only the top plane.
2. In addition, the interactions can be governed by the van der Waals force but also by strong covalent bonding. All these kinds of interactions can perturb the electronic system of graphene, which can be monitored by suitable electronic methods.
3. Thanks to other electrical and structural properties, such as the charge carriers zero rest mass near the graphene Dirac point, the remarkable high carrier mobility at room temperature up to 200.000 $cm^2\ V^{-1}\ s^{-1}$, the extremely low resistivity of $10^{-6}\Omega$cm and its high-quality crystal lattice along with its two-dimensional structure (see Chapter 2), a small amount of extra electrons can produce strong changes of the graphene physical properties during the interaction with the different substances even down to the molecule level.

Apart from these unique properties and the high sensitivity, the focus and growing interest for the gas sensing application is also due to the graphene mechanical flexibility, to its technological compatibility with metals and semiconductors, allowing to realize various types of devices, e.g. Schottky hetero-junctions, and, not least, especially to the strong stability in environmental conditions at RT [10, 29, 37, 42, 53, 70, 80, 82].

1.4 Goals and outline of the thesis

The goal of this research is twofold: firstly, I will present and compare graphene realized by different synthesis techniques, carrying out a study on the material; then, analyzing the sensing properties of the materials produced in the different routes, I will report on graphene-based transducers towards analytes.

Apart from the present Chapter that serves as introduction to the thesis, the two major items will be split into four sections which can be summarized as follows:

- ✓ an overview on the various methods for the graphene synthesis is faced up in the **Chapter 2**, with a particular focus on the routes mostly used in this research, that are Liquid Phase Exfoliation (LPE) and Chemical Vapor Deposition (CVD). A comparison between these two methods is performed with the aim to find advantages/disadvantages for the gas sensing application and, finally, a quick look at the role of defects for the same purposes is given;
- ✓ the **Chapter 3** is totally devoted to the experimental results on the material synthesized by LPE and CVD. I pay particular attention to the material characterizations that I have performed via Raman spectroscopy, Atomic Force Microscopy (AFM) and Transmission Electron Microscopy (TEM), in order to check the quality of such prepared graphene. These analyses are focused to optimize the recipes for the material preparations, aimed to improve and make the performances of graphene-based gas sensor reproducible.
- ✓ the **Chapter 4** pertains a chemi-resistor based on LPE graphene, the first type of employed sensor. Starting from the device realization, a brief dissertation on the slow and incomplete recovery after the signal detection is presented. However, this bottleneck paves the way to a new approach to overcome the problem, using the derivative of the signal output instead of the signal itself. It reveals so powerful to allow the calibration of the sensor towards NO_2 concentrations, as discussed in the last part of the chapter. Herein the comparison with the chemi-resistor based on CVD graphene is addressed with the aim to better understand the sensing properties of the material prepared in two different ways.
- ✓ In the last part of the Thesis, there are **three appendices**: **the first one (Appendix A)** provides the details of alumina substrate employed for the chemi-resistive sensor which has been dealt with in Chapter 4; **Appendix B** is

dedicated to the equipment description for the sensor tests and **Appendix C** is a summary of all the abbreviations and acronyms met in the text.

CHAPTER II

ROUTES FOR GRAPHENE PREPARATION

In this Chapter, an up-to-date overview regarding the various methods for the graphene synthesis is discussed, spending few words more for the routes mostly used in my research, i.e. Liquid Phase Exfoliation of Graphite and Chemical Vapor Deposition. The two methods are compared in order to present the behavior of so prepared material for the gas sensing application. The section concludes reporting on the material structural defects and explaining the effects of the defects in the adsorbates detection.

2.1 The graphene preparation methods: an overview

Starting from the simply definition of GR (see Chapter 1), an ever seen growing research effort has been developed in the last decade. To understand the trajectory and the aim of research on the material, it is useful to consider GR as simply the fewest layer limit of graphite. Generally speaking, this is the basic idea underlying the so called GR production approach "top-down", while the opposite idea is the basis of the "bottom-up" approach. The main difference between the two approaches consists basically in the starting point: the former starts from graphite, then single layer is obtained by its exfoliation, while the latter starts from other materials, such as carbon precursors (methane, ethane, acetylene), to epitaxially grow the single layer on top of suitable substrates at the end of the process.

The following flow charts (Fig. 2.1) depict the two typical approaches and some of the most known families for the GR production techniques, that will be shortly described in conclusion of this paragraph and within the next one.

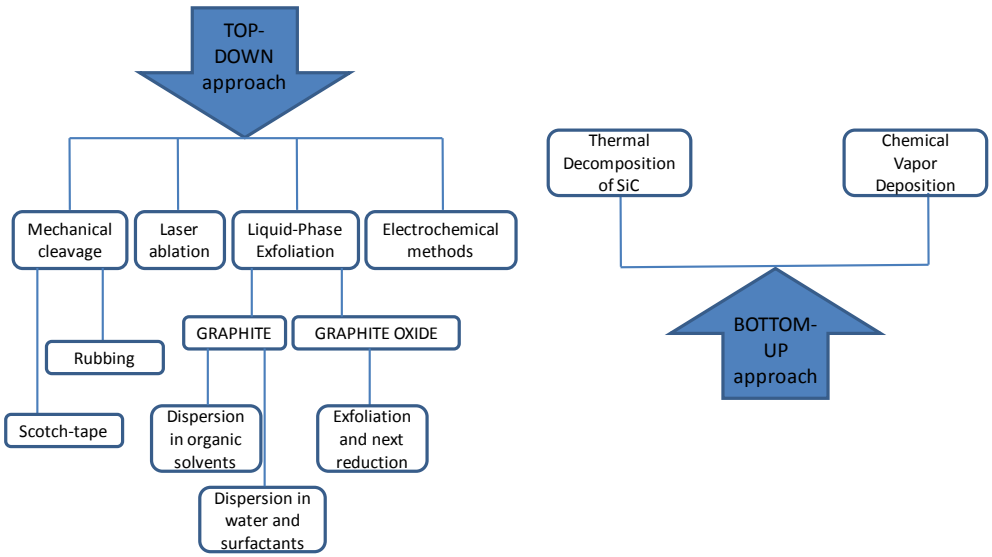

Fig. 2.1: schematic pictures reporting both the approaches top-down and bottom-up as well as the methods for graphene production belonging to these families.

Catching eyes from Fig. 2.1, an immediate difference regards the plentiful number of the top-down techniques with respect to bottom-up ones. The fact can be easily explained by considering the major equipments cost, also taking into account the maintenance costs for the bottom-up approach, e.g. of a reactor for the Chemical Vapor Deposition (CVD), with respect to the experimental structures used for the other methods, in some cases even not necessary; for example, to perform mechanical cleavage only adhesive tape and a small block of Highly-Oriented Pyrolitic Graphite (HOPG) are required [37].

As a matter of fact, to date all these methods have revealed particularly useful for pure lab research. The key requirement to jump from this step to technological applications, making GR even more appealing for the industry, lies into the development of industrial-scale, reliable and not expensive production processes. Also, the most challenging issue for mass-production is to obtain outstanding quality comparable with that of material produced in the research lab.

When scientists cite the material quality, generally they refers to the GR characteristics, that are the electrical, optical, thermal, mechanical and some other physical properties. In Table 2.1 some of them are summarized with the respective values.

GRAPHENE	OTHER MATERIALS	REFERENCE VALUES

Mobility (@ RT)	$10^3 \div 10^5$ cm^2 $V^{-1}s^{-1}$ [70, 80, 82]	Copper	32 cm^2 $V^{-1}s^{-1}$
	$2 \cdot 10^5$ $cm^2V^{-1}s^{-1}$ (suspended graphene) [66]		
Resistivity	$1.0 \cdot 10^{-8}$ Ωm [51]	Silver	$1.59 \cdot 10^{-8}$ Ωm
Conductivity	$10^5 \div 10^8$ S/m [4]	Silver Copper Gold	$6.30 \cdot 10^7$ S/m (@ 20 C) $5.96 \cdot 10^7$ S/m (@ 20 C) $4.10 \cdot 10^7$ S/m (@ 20 C)
Current density	$>10^8$ A/cm^2 [81]		
Transmittance (VIS)	97,7% [59, 60]		
Young Modulus	1.02 TPa [61]	Diamond	0.82 TPa
Thermal Conductivity (freestanding)	4800-5300 $Wm^{-1}K^{-1}$ [62]	Diamond	1000-2200 $Wm^{-1}K^{-1}$
Thermal Conductivity (on substrate)	600 $Wm^{-1}K^{-1}$ [48]	Silver	430 $Wm^{-1}K^{-1}$
Carrier density	~10^{12} cm^{-2} [70, 82]		

Table 2.1: graphene physical properties and respective values reported in literature.

Noteworthy, the most part of the reported values have been obtained in experimental works involving GR flakes realized by micromechanical exfoliation (ME) to confirm the quality of as-prepared material. To better validate this assessment, it could be relevant to analyze the following sketch (Fig. 2.2), picturing schematically some of the above mentioned synthesis methods.

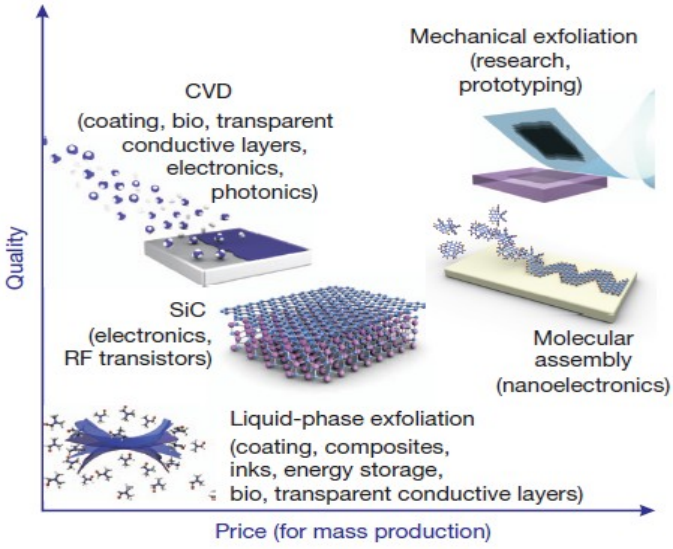

Fig. 2.2: sketch reporting level of graphene quality versus production costs for the different techniques (ref. [29], © Nature 2012)

Fig. 2.2 also reports the quality of material versus the costs for scalable production. It is well known that ME remains the best method for the highest quality GR production, primarily because it benefits from the high-quality of the starting single crystalline graphite source (HOPG). Unfortunately, this procedure, resulting a little bit laborious, is affected by a series of limits, such as poor flakes yield, random location of the GR pieces on the substrate and flakes mean size in the order of hundred micron square [37]. Hence, it is challenging and simultaneously expensive to bring this approach to large scale production level but surely it will remain the best for the fundamental studies, for the prototypes realization and it will provide the standard to reach for the GR prepared in the other ways [37, 51, 65-67, 70].

On the contrary, Fig. 2.2 shows that Liquid Phase Exfoliation (LPE) allows to produce material with not so high quality. This could be also true if as-prepared GR is compared with that one produced by ME, but LPE represents one the most promising tools for mass production, permitting to reach an excellent trade-off between the scale-up and the production costs. Furthermore, LPE GR is notably fit for some applications [29, 32], e.g. gas sensing, as it will be proved in this thesis. In general, in fact, it is important to keep in mind that: *1)* the choice of the production method will certainly depend on the specific application; *2)* GR films on large-scale

could present different physical properties with respect to smaller ones prepared by the same methods.

CVD growth, instead, is considered not only as the most promising candidate able to improve the quality up to ME GR one on large scale but also, thanks to its flexibility, it can serve as a launching pad for other 2D layered and chemically tuned materials, such as hexagonal boron nitride films (h-BN) or transition metal dichalcogenides (TMDCs) such as molybdenum disulphide (MoS_2), tungsten sulphide (WS_2), niobium diselenide ($NbSe_2$), simply by changing gas sources [29, 33, 47]

In the following, I am going to shortly inspect the aforementioned methods, starting from the bottom-up approach and continuing with the top-down one. In particular, CVD and LPE of graphite, that are the mostly exploited techniques for the material production in this work, will be more widely discussed.

2.1.1 Chemical Vapor Deposition

CVD is a process widely used in semiconductor industry to deposit or grow thin films, crystalline or amorphous, from chemical precursors of many materials in the vapor phase. The choice of precursors usually depends on the composition of the desired film and what is the effective cost for the specific application. Various types of CVD processes exist: thermal, plasma enhanced (PECVD), cold wall, hot wall, reactive, and many more. One or another type can be chosen according to available precursors, the material quality, the thickness and the structure needed, strictly jointed to the cost of selecting a specific process [29, 32].

The thermal CVD is one of the most used types for the GR growth. The first attempt dated back to 1966 when Ni substrate was exposed to methane (CH_4) at T = 900 °C to form thin graphite. In the last years, not only other gaseous hydrocarbon sources, such as acetylene or ethylene, but also Cu and other transition metals have been introduced while more recently also Mo has been successfully tested [5].

The growth mechanism can be easily understood analyzing the following diagram (Fig. 2.3), reporting a typical process sequence.

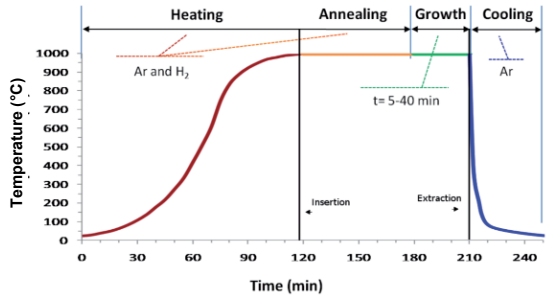

Fig. 2 2: typical process cycle of GR growth on Cu displaying the temperature profile as time function.

The process relies on carbon saturation of a transition metal during the exposure to a hydrocarbon gases at high temperature. The substrate cooling determines the decreases of carbon solubility in transition metal with a consequent carbon layer precipitation on the surface. The catalyst substrate is put in a chamber able to reach high temperatures around 1000 °C depending on the substrate and, under a continuous flow of carrier gases, the sample is gradually heated up to the growth temperature. After flowing the reaction gas mixtures, the carbon atoms, that decompose from hydrocarbons due to the high temperature of the substrate,

nucleate on the catalyst substrate itself and the nuclei grow into large domains. The last step, that is critical in suppressing formation of multiple layers and for separating GR layers efficiently from the substrate, regards the rapid cooling of the substrate in inert atmosphere to RT [47, 58].

The nuclei density is principally a function of T and pressure and, when the catalyst surface is fully covered, the films become polycrystalline, since the nuclei are mis-orientated with respect to each other, even on the same catalyst grain. This issue represents the first hindrance to obtain a continuous layer [32]. The second one is the removal and transfer process from the growth substrate to the target one, this phase being the most critical and tricky in the manufacturing of GR produced by CVD. In general, graphene is transferred from one substrate to another using either *a)* the carrier method or *b)* the stamp method.

a) In the carrier method, a thick organic film, typically poly(methyl methacrylate) (PMMA) or polycarbonate (PC), is required to incorporate GR grown on the substrate. After the substrate is etched away, the resulting stack is placed on top of the target substrate and finally the carrier film is removed by chemical or thermal treatment [15].

b) In the stamp method, an elastic and sticky film like polydimethylsiloxane (PDMS) is required to attach the GR sheet on the growth substrate. This is then etched away with GR/stamp sandwich that is stamped on top of the target substrate. Finally, the stamp is removed by mechanical detachment similar to slow peeling off [15-16, 43].

Albeit outstanding improvements have been obtained, both of these methods can provoke damages or cracks, resulting in discontinuous films. Nevertheless, some research groups have been able to produce large scale foils. For example, Hobara et co-workers have recently reported on the fabrication of GR films one-hundred m long with physical properties fairly comparable with those of state-of-the-art CVD-grown graphene films [11]; also Bae et al., in 2010, achieved a similar result producing 1m roll-to-roll graphene films for transparent electrodes [45]. This means that the mass and scaled-up production of CVD grown GR is a possible and almost a reached goal.

2.1.2 Thermal decomposition of silicon carbide

The preparation of GR by the thermal decomposition of silicon carbide (SiC), sometimes indicated also as SiC segregation, has been proposed as one of the viable routes for the synthesis of uniform and large-scale GR layers [56]. The method of producing graphite from SiC is known as early as 1896, as reported by Acheson [32].

Growth of GR on SiC is usually referred to also as "epitaxial growth", where the term "epitaxy", deriving from the Greek, is formed by the prefix "epi", which means "over" or "upon", and "taxis", which means "order" or "arrangement". Actually, there is a considerable lattice mismatch between SiC (3.073Å) and GR (2.46 Å) and, differently from what happens in a traditional epitaxial growth process, in which Si is deposited on the SiC surface, in this growth technique the carbon rearranges itself in a hexagonal structure after the Si evaporation from the SiC substrate [32].

The procedure for the SiC thermal decomposition is theoretically simply and consists basically of two steps: firstly the samples cleaning is required to remove surface polishing damage, then the growth starts by thermal treatment of SiC.

Regarding the first step, various approaches have been adopted: Rollings and co-workers, for example, polished the SiC surfaces in situ by annealing up to 850°C under silicon flux for 20-30 min [77]; Emtsev et al., instead, etched the samples in hydrogen (grade 5.0, p=1 bar, T=1550°C) for 15 min [56].

For what concerns the second step, the annealing of the substrates results in the sublimation of the silicon atoms while the carbon-enriched surface undergoes reorganization and, for high enough temperatures, graphitization [51]. The typical range of annealing temperatures goes from 1300°C to 2000°C and the usual heating and cooling rates are 2-3°C/sec, although Sodano et al. reports on that the quality of GR is improved by operating at 1650 °C under argon rather than at 1150 °C in ultra-high vacuum (UHV) [51, 56].

This technique allows to obtain, to date, GR domains up to 200 nm in size with mobility at RT up to $3 \cdot 10^4$ $cm^2V^{-1}s^{-1}$. The thermal decomposition, however, is not a self-limiting process and areas of different film thicknesses may exist on the same SiC crystal but the major short-coming regards the SiC wafers cost that blocks up the breakthrough of this method. A considerable advantage for the technological

applications is that SiC, being an insulating substrate, can be simultaneously used as growth and election substrate without transferring the graphitic layers to another insulator substrate, avoiding all the drawbacks due to this process, as will be discussed later, for example, for the CVD technique [32, 56].

2.1.3 Mechanical cleavage

The mechanical cleavage or exfoliation can be regarded as the mother of all techniques for the GR production, since it was the way that allowed Geim and co-workers at Manchester University in 2004, to isolate the first single-layer samples from graphite [82].

It consists basically in the exfoliation of a graphite block, HOPG or other types, through the adhesive tape so that the method has been universally known as "the scotch-tape technique". Then, the first piece of tape is repeatedly cleaved by other sticky pieces down to obtain an almost invisible powder on the starting tape[3]. The number of the exfoliations ranges from 10 to 20 but, as I demonstrated in ref. [37], a trade-off between this number, namely the flake thickness, and the mean size needs to be reached. Finally, at the end of the exfoliation process, the tape is transferred onto the election substrate that usually is silicon dioxide on Si (SiO_2/Si) [37].

As I said before, it is clear why this procedure is proposed as the origin of the top-down approach: ideally, in fact, the single-layer graphene (SLG) can be obtained making thinner and thinner the thickness of the graphite block.

However, transferring the adhesive tape to the SiO_2/Si implicates that also glue residues can be released on the substrate. Because the residues make the GR optical identification and the samples processing more difficult, e.g. by photolithographic methods for the devices production, several attempts have been done. Among these, for example, I was spurred to improve the "scotch-tape technique" replacing the scotch with something less sticky than scotch. A thermo-curable elastomer, called polydimethylsiloxane (PDMS) resulted to be extremely suitable to the aim and the introduced variant, that I named PDMS-film technique, besides eliminating the glue residues, was able to increase the mean flake size from ten up to hundred of microns [37-38]. Unfortunately, the bottlenecks related to the mass production are always confirmed but, as discussed before, once more time it appears the best avenue for the pure lab research.

[3] In some cases, instead of exfoliating continuously the first piece, the last piece of the tape series is subsequently folded down to obtain, at the end, an almost invisible powder at naked eye on the tape.

2.1.4 Electrochemical methods

In the class denoted as electrochemical methods the most used one relies on the anodic bonding (AB) which may be classified as a variant of mechanical cleavage. AB is widely used in the microelectronics industry to bond Si wafers to glass, to protect them from humidity or contaminations, but also for joining glass to conductive material, the two materials being fairly well matched in terms of thermal expansion (silicon-on-insulator bonding or SOI bonding) without intervening glue or others sticky resins [52].

AB is achieved by pressing borosilicate glass on a Si wafer at high temperatures, above 200°C, while a high voltage, typically in the range 1700–1800V, is applied perpendicular to the layers. The heating makes decompose the Na_2O impurities in the glass into Na^+ and O^{2-} ions and the mobility of the lighter sodium ions is higher than that of O^{2-} ones. The voltage polarity is chosen so that the Na^+ ions can migrate away from the Si-glass interface to the back contact, leaving behind a negative space charge in the region of the interface formed by the static oxygen ions remained there. Since the space charge layer is typically a few hundred nanometers to a few micrometers thick, the field created across this layer is very strong and pulls the wafer into contact with the substrate, ultimately leading to the formation of stable Si–O–Si bonds and resulting in a wafer bonded to the glass substrate. When employing this technique to deposit GR, graphite replaces the Si and the same above described procedure is followed. The typical time of potential difference application is 10-20 min. At the end, when the bonding is achieved, the bulk graphite sample can be peeled off, using either a scalpel blade or adhesive tape or both and leaving onto the glass many transparent areas with one-layer, or few-layer GR portions. It should be noted that all these steps are performed in standard laboratory environment, there being no need for a controlled, clean room atmosphere, exactly as happen for ME [52, 57]. This requirement represents an important added value for the technique that, despite the simplicity of the employed setup, has been rarely adopted mainly because it allows depositing graphene on substrates with relatively mobile ions, such as borosilicate glass. This substrate is useful to study the optical properties of GR, but it is not particularly suitable for other kinds of studies, such as transport measurements, because of the lack of backgate. On the other hand, AB prepared material has quality as high as that

prepared by ME, as confirmed by Moldt et al. in ref [92], where they have obtained charge mobility of so-prepared flakes on the order of 6000 cm^2V^{-1} s^{-1}, which is fairly comparable with devices prepared with exfoliated GR. Therefore, similarly to ME, AB technique permits to obtain GR of superior quality with an extremely low yield of SLG and FLG and mean flakes lateral size in the range of few hundred micrometers.

2.1.5 Laser ablation

The basic idea underlying the laser ablation GR growth technique is the same mostly adopted for the cure of the monuments or works of art since the ablation generally serves to remove material from a solid surface through the laser beam. If irradiation results in the detachment of an entire or partial layer, the process is called photoexfoliation [32].

In the case of GR growth, the material that is usually ablated is HOPG and the laser mainly used is the neodymium-doped yttrium aluminum garnet (Nd:YAG). [39-40, 72]. Keeping fixed the laser pulse rate, the growth substrate and the HOPG sample, as target wafer, are loaded in a vacuum chamber. The laser energy density tuning is the parameter that mainly affects the ablation and consequently the deposited number of GR layers (nLG). In fact, Qian et al., exploiting a laser energy density windows, have observed the variation in the nLG as well as the different nature of the deposited material, involving amorphous carbon, FLG and thin graphite films [40].

Although the process is still in its infancy and needs further developments, it has the interesting potentiality to allow the deposition of graphene nanoplatelets on arbitrary surfaces. Also, besides the PDMS-film technique, it provides an alternative route to solve the glue residues problem reported about the ME technique. On the other hand, the main short coming is that it reveals not particularly suitable for mass-production since the mean flake lateral size is around ten microns [40].

2.1.6 Liquid Phase Exfoliation of Graphite Oxide

The chemical routes for GR production appear to be the most viable alternatives to the other methods. In order to address this issue, there are two main chemical ways to do this: oxidization of graphite followed by exfoliation in water to give graphene oxide and exfoliation of graphite in solvents or surfactant solutions to give dispersed GR flakes (see next paragraph). Notably, both of them are real cost-effective methods for mass-producing graphene, but it is important to keep in mind the trade-off already discussed in Paragraph 2.1 and the applications to be addressed.

The first method consists in producing chemically modified GR, such as graphene oxide (GO), according to the Hummers method, successively reducing into GR [90]. Large-quantity of GO can be easily produced by the chemical exfoliation of graphite through oxidation and the subsequent dispersion in water. The oxidation of graphite in the presence of acids and oxidants disrupts the sp^2 network and introduces hydroxyl or epoxide groups with carboxylic or carbonyl groups attached to the edges and to the basal plane. In this way, GO sheets become readily dispersible in water and in several other solvents. Even though large flakes can be potentially obtained, GO is electrically insulating, does not possess the GR properties and it is also conceptually different from GR. GO needs to be processed in order to significantly increase the electrical conductivity, owing to the presumably restoration of the sp^2 bonds. This can be achieved by exposing GO to reducing agents such as hydrazine, NaBH4, through high-temperature treatment or via UV-assisted photocatalysis and so prepared material is generally identified as reduced graphene oxide (rGO) [29, 50, 74, 93].

However, several attempts show that, besides being hazardous and enough aggressive methods for the environment, it is quite impervious to make rGO regain the pristine GR electrical conductivity because of the significant presence of many structural defects introduced by the oxidation process that continue to disrupt the GR band structure. On the other hand, rGO presents the advantages that it can be deposited on different substrates and, thanks to the presence of functional groups which favors the link with polymers, is ideal for nano-composites preparation [32, 75].

2.1.7 Liquid Phase Exfoliation of Graphite

Liquid-phase exfoliation of graphite is based on exposing powdered graphite to special solvents or surfactants that favor an increase in the total area of graphite crystallites [34, 44]. Solvents ideal to disperse graphene are those that minimize the interfacial tension [mN/m] between the liquid and GR flakes, i.e. the force that minimizes the area of the surfaces in contact [3, 32]. The solvents that mainly match this requirement are N-methyl-pyrrolidone (NMP), Dimethylformamide (DMF) and others Lewis bases [68].

The second step of the procedure consists in the ultra-sonication aimed to favor the splitting of graphite into individual platelets. Finally, a "purification" step is required to separate the unexfoliated flakes from the thinner ones, constituting the so called surnatant phase of the suspension. Thicker flakes can be removed by different strategies based on ultra-centrifugation in a uniform medium or in a density gradient medium [32].

Because this technique is regarded as one of the most promising tools for mass production, high concentration is desirable so that the main research efforts are addressed to improve the SLG-FLG yield in the dispersion. The yield is usually defined as the ratio between mono- or few-layers and the graphitic flakes in the dispersion. To this regard, it is important to note how the yield and accordingly the final result is strongly affected by each parameter involved in the three steps of the procedure: for example, Khan et al. have proved that, increasing the mild sonication time, they are able to obtain concentration 100 times higher than that reported in literature [44]; similarly, increasing the sonication time from 3h to 168h for material prepared in NMP, we have observed a series of beneficial effects related to a better exfoliation of graphite, a higher concentration of FLG as well as a larger lateral size of FLG, as will be better discussed in the next chapter; also, ref [32] reports that the sonication power can dramatically influence the flakes size because of the in-plane fracture.

In conclusion, these intrinsic drawbacks are counterbalanced by much heavier assets: the cheapness, the easy scalability and the absence of expensive growth substrates. More importantly, LPE reveals particularly suitable for a large range of applications and to produce inks, thin films, and composites; the versatility of such preparation technique displays in the ability to deposit the GR on rigid and

flexible substrates by several approaches, such as drop and dip casting, rod coating, spray coating, screen and ink-jet printing and other techniques discussed in ref [32]. Finally, LPE as well as CVD can be also adapted to produce other layered materials and TMDCs [29].

2.2 A challenge for sensing

All the definitions associated to GR generally refer to the ideal structure, but the films usually prepared by means of the various methods might be different from the ideal case and they can contain defects. In Physics, the term "defect" identifies anything that breaks the symmetry, in this case the symmetry of the infinite carbon honeycomb lattice. Hence, in GR sheets a plenty of defects can be observed such as edges, grain boundaries, vacancies, implanted atoms and the defects associated to a change of carbon-hybridization, for example, from sp^2 into sp^3 [28]. It is remarkable to note that some of these, albeit impossible to remove, as happens for the films edges due to the impossibility to obtain infinite sheet, do not represent a drawback; on the contrary, deviations from perfection can have a strong influence on the GR electronic, optical, thermal, mechanical and sensing characteristics making possible to tailor the local properties of GR and to achieve new functionalities, like in conventional semiconductors [63, 94]. In addition, GR, differently from the conventional 3D materials, is the ideal means to study defects because its planar nature allows easily to add, remove or move carbon atoms and accordingly modify the basal structure [28]. The case of interstitial atoms, as they appear in 3D crystals, for example, cannot exist in GR because placing an atom to any in-plane position would require a prohibitively high energy. Therefore, obeying to energetic considerations, the additional atoms use the third dimension and the energetically favored position is the bridge configuration on top of a C-C bond [46]. At first glance, the presence of this additional not-conjugated atoms in the defected GR configuration makes clearer why the sensing properties of the sheet could be improved so that it becomes more prone to the sensing application with respect to the pristine one.

As far as the defects generation is concerned, there are basically three mechanisms which can produce defects in GR, that are: *1)* the crystal growth, 2*)* the irradiation with energetic particles, for example, electrons or ions, and 3*)* the chemical treatments [26, 46].

1) The defects originating from the growth techniques, firstly are generally present on GR grown via techniques on large-scale, secondly are due to the intrinsic way of the layers growth. A GR layer, in fact, does normally not occur atom-by-atom from one nucleus but rather as a relaxation of a metal carbon system

with many nuclei, e.g. in CVD, determining, in this way, the rise of a no perfect crystal lattice.

2) Irradiation beams lead usually to a generation of point defects whilst an uniform irradiation of large areas can produce randomly distributed vacancies. Also focused ion beam (FIB) can generate vacancies in the lattice with the difference that preselected positions can be stricken by the highly focused gun.

3) As regards the chemical treatments, the reactions occurring between carbon atoms in a GR layer and other species can provoke the loss of atoms and thus the defect production. One of the most common reactions involving GR at RT is the oxidation that usually happens with oxidizing acids, such as HNO_3 or H_2SO_4, for example during the transfer of CVD grown GR from the catalyst substrate to the insulating one. Such treatment can allows to attach oxygen and hydroxyl (OH) or carboxyl (COOH) groups to GR.

As discussed before, all types of defects can contribute to improve the GR properties, as reported, for example, in ref. [22] regarding the thermal transmission. In the sensing field, particularly, the role of defects has been deeply investigated, above all from a theoretical point of view. Numerous simulations have shown, in fact, that defects associated with dangling bonds should enhance the reactivity of GR, in particular OH, COOH or other groups can easily be attached to vacancy-type defects. The same is equally true for GR edges that are normally saturated with hydrogen [55, 63].

The enhanced effects of defects for GR sensing properties is also confirmed by Zhang and co-workers [54]. They report on a first-principles simulation of the interactions between several small molecules and various GR sheets, i.e. pristine, p-, n-doped and defected GR. The results show that the adsorption of three over four considered molecules is favored over the defected GR in comparison with the other kinds of sheets.

In addition, several experimental works provide proofs of this concept. Salehi-Khojin's group [27] demonstrates that deliberately defected GR-based sensors not only show higher response in comparison with defects-free GR but also the combination of different kinds of them, such as line and edge defects, improves the response much more than edges or line defects alone. In ref. [36, 64] the authors analyze GO and rGO-based gas sensors, respectively. As discussed before, GO contains oxygen functional groups such as epoxides, alcohols, and carboxylic acids

determining a strong defected structure as well as rGO that has not only chemically active defect sites but also partly the honeycomb sp^2 structure. Both the papers describe two regimes in the response curve upon the gas exposure: a faster and a slower one. These phenomena are easily understood by attributing the fast response to the molecular adsorption onto binding sites with low energy, such as sp^2-bonded carbon, while the slow response is due to the interactions between gaseous molecules and high-energy binding sites such as vacancies, defects, and oxygen functional groups.

To conclude, this brief survey clearly suggests that:

1. in the sensing field, defected GR, being more reactive towards molecules, seems to be more suitable for the gases detection;
2. because it is practically impossible to obtain defects-free GR, even simply because the sheets are finite and edges or grain boundaries are considered defects, a avenue could be to increase intentionally the creation of defects offering a means for improving the GR sensing performances;
3. provided that edges and grain boundaries can be extremely useful for sensing, in this field the GR flakes dimension does not seem to be an essential requirement, because ideally the more the flakes are small the more the edges are present.

CHAPTER III
MATERIAL PREPARATION AND CHARACTERIZATION

In this Chapter, the optimized procedures for the GR synthesis by LPE and CVD are described. The characterizations performed through Raman spectroscopy, Atomic Force Microscopy and Transmission Electron Microscopy are also presented. The experimental results, compared with those reported in the literature, allow to argue the morphological and structural nature of such prepared materials. The issue regarding the GR defects is also addressed with the purpose to better understand the strong sensitive of material in the sensing field.

3.1 Liquid Phase Exfoliation: the procedure

As discussed in the previous chapters, the LPE technique belongs to the top-down approaches and basically consists in the separation of the graphite planes through the energy provided by the sonication of graphite previously dispersed in the solvents. However, the mostly used solvents are characterized high boiling points (>450 K), are expensive and require special care in handling due to their toxicity; e.g. NMP may be toxic for the reproductive organs, while DMF may have toxic effects on multiple organs [3, 68]. In particular, the high boiling point can negatively affect further processing of the material, such as to the solvent removal after the exfoliation and the deposition of individual flakes due to their aggregation during the solvent slow evaporation. These circumstances make advisable the recourse to green solvents. In addition, these approaches will be highly regarded since the availability of high quality GR dispersions in the most environmentally friendly solvent, i.e. water, could pave the way to the use in a wider range of applications [3].

Among the thermodynamic properties related to the solvent solubility capabilities, the key role in the process is attributed to the solvent surface tension (γ) so that, the closer to the graphene (around 40 mN/m) the solvent

surface tension value is, the more effective the exfoliation is. As a matter offact , water, the “natural” solvent, has γ ~72 mN/m that is both too high for the GR dispersion and about 30 mN/m higher than NMP [32].

Therefore, by analyzing the solvents thermodynamic properties and the physicochemical parameters, we have successfully addressed a green mixture of iso-propanol (IPA) and ultrapure water in volumetric ratios 1:5 having a surface tension value suitable to achieve the target value of ~40 mN/m and, especially, able to exfoliate graphite. The optimized recipe for the colloidal suspensions preparation consists in dispersing graphite flakes (Natural Graphite) at 2.5 mg/ml and sonicating in an ultrasonic bath for about 48h with power set at about 40 W. The “purification” step aimed to separate unexfoliated graphite from the thinner flakes has been carried out by the suspension centrifugation for 45 min at 1000 rpm [3].

The achievement of this result has twofold relevance: besides developing a new mixture able to directly exfoliate graphite, more importantly the solutions so prepared have been demonstrated to be stable with yield in few layer graphene content and flakes quality fairly comparable with those obtained using NMP, as I will deeply discuss in the following.

3.2 Characterization of LPE graphene

The first characterization on the GR suspension is conducted through Dynamic Light Scattering (DLS), mainly devoted to determine the dimension of the platelets. This analysis, performed by means of NanoZetasizer (Malvern Instrument), has revealed a mean flakes lateral size of (430±10) nm and (260±30) nm for suspensions prepared in H_2O-IPA and NMP, respectively. Analogues results have been collected at later times, confirming the stability of such prepared GR solutions [3-4].

Afterwards, Raman spectroscopy is performed on GR films. This non-destructive technique, particularly useful for all carbon allotropes, represents an extremely versatile tool for studying all GR properties, allowing to obtain structural and electronic information, and can be applicable at both laboratory and mass-production scales [20]. In other words, through the Raman spectrum, the complete GR fingerprint can be depicted.

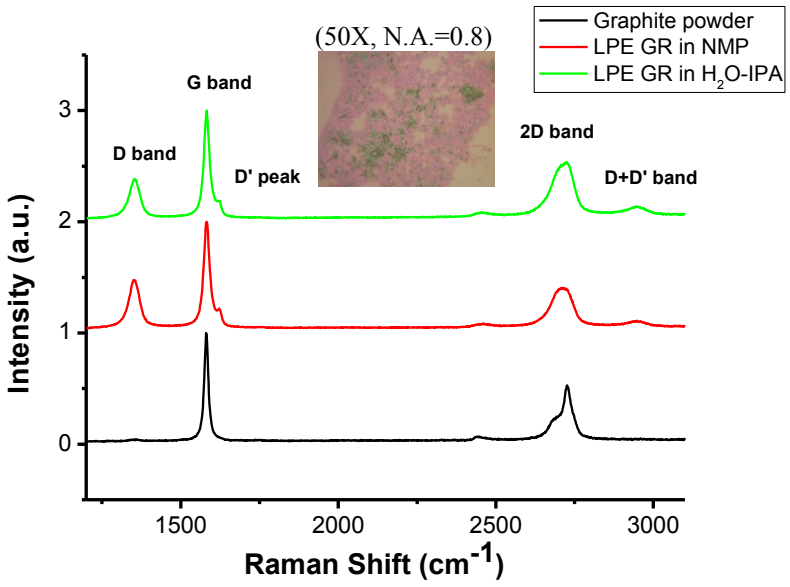

Fig. 3.1: typical Raman profiles for LPE GR exfoliated in NMP (red line) and in H_2O-IPA mixture (green line); the black line shows the graphite spectrum. All proper graphitic bands in the explored range are labeled. Inset: an optical image of graphene film.

The Raman measurements herein presented have been performed depositing few microliters of the feed solution onto Si wafers coated with SiO_2 thin film (250

nm). The inset in Fig. 3.1 shows a GR film picture taken under the optical microscope.

The spectra have been captured through a Renishaw inVia Reflex apparatus in back-scattering configuration by using the 514.5 nm line of Ar laser as excitation source with an incident power of ~10 mW and a magnification 100x.

The typical Raman profiles for LPE GR, prepared by using NMP (red line) and H_2O-IPA (green line) as solvents, are shown in Fig. 3.1, in comparison with the graphite spectrum (black line). The distinct graphitic bands in the explored range are labeled and, in order to facilitate the visualization, all spectra have been normalized to the G band intensity [20-21]. The G peak corresponds to in-plane vibrations at Γ, whereas the breathing mode of the six-atom ring gives rise to the D peak and requires a defect for its activation. The D' peak originates from a double resonance intravalley process which also activated by a defect. Therefore the intensities of D and D' peaks are closely related to the amount of defects in the GR lattice. In contrast, the 2D peak (overtone of D-peak) and the 2D' peak (overtone of D'-peak) are both activated without requiring the presence of defects and are thus always present.

By comparing the graphite spectrum (black line) with the others two (red and green lines), some indications of the successfully graphite exfoliation are well rendered: firstly, the rise of D (~1350 cm^{-1}), D' (~1620 cm^{-1}) and D+D' (~2900 cm^{-1}) peaks, then the change of the 2D band (~2700 cm^{-1}) shape. The remarkable overlapping of the two spectra related to GR (green and red lines) represents a first confirmation of the equivalence between the different solvents in the direct exfoliation of graphite.

As regards the D and D' peaks, an in-depth speech will be done later, whereas the 2D band features are examined in Fig. 3.2[4]. The lower and the upper panels refer to graphite and exfoliated material, respectively. To perform the following comparison, the spectrum of the exfoliated material has been captured in another point of the film deposited onto the SiO_2/Si substrate.

[4] This analysis is conducted on the material prepared by using NMP solvent due to the substantial equivalence to GR exfoliated in H_2O-IPA.

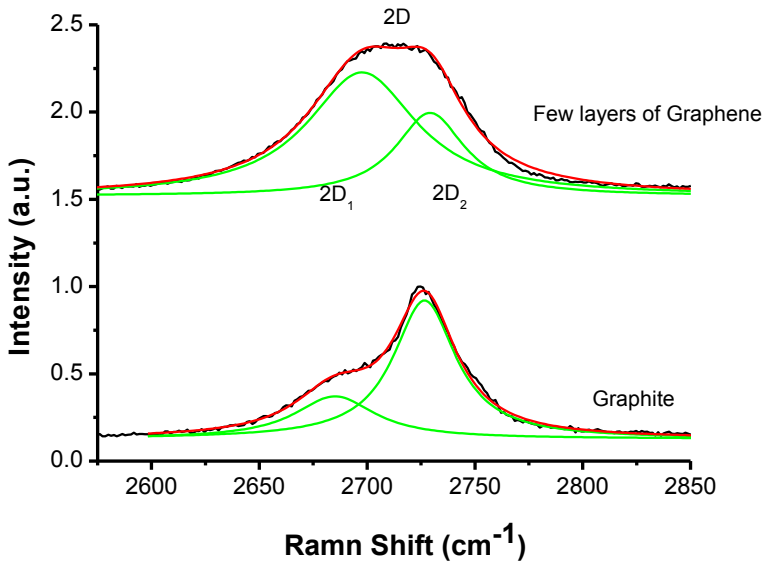

Fig. 3.2: Zoom on the 2D band of graphite (lower spectrum) and oligolayered graphene (upper spectrum). Both spectra are normalized to the 2D intensity. The deconvolution of the 2D band is reported as green line, while the black and red lines report the profile and the two components sum, respectively. In both panels, the two components are quite distinguishable as well as the evolution from graphite to oligolayered graphene.

As demonstrated by Ferrari et al. [76], the 2D band of graphite consists of two Lorentzian components, $2D_1$ and $2D_2$, centered roughly at 2695 cm^{-1} and 2735 cm^{-1}, respectively (green lines in the lower panel of Fig. 3.3), with the $2D_1$ less pronounced than the $2D_2$. As the number of graphene layers decreases and reaches the limit of five, the relative intensity of the $2D_1$ peak increases progressively and $2D_1$ shifts towards $2D_2$ peak (upper panel in Fig. 3.3), until it becomes, in general, the only component in SLG. During this evolution, the 2D band becomes smoother and broader and, in presence of SLG, the 2D band can be fitted with a single, sharp Lorentzian as reported, for example, in ref. [21]. In our work [2] this behavior can be argued and the full-width at half maximum (FWHM) is estimated equal to about 70 cm^{-1}. Indeed, because FWHM is higher than 25 cm^{-1}, corresponding to SLG, a further validation of the evolution from graphite to FLG is provided.

Finally, Fig. 3.3 reports five spectra for material exfoliated in NMP (Fig. 3.3a) and in H_2O-IPA (Fig. 3.3b). The intensities, normalized to the G band, have been averaged on ten values collected in different points of the films.

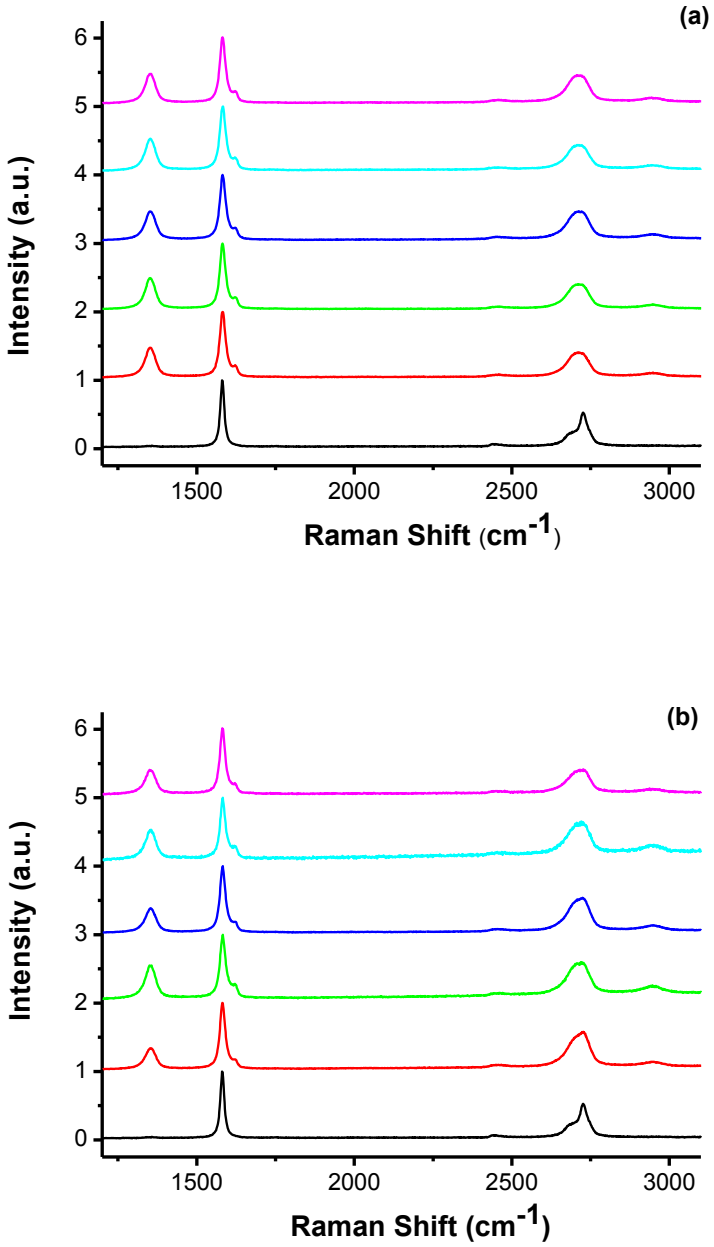

Fig. 3.3: spectra of FLG exfoliated in (a) NMP and (b) H_2O-IPA. Each profile is determined as the average of the spectra taken in ten different points of the film. The black profile refers to the graphite flakes.

In each family, comparing the spectra, a fairly reproducibility can be observed, justifying the homogeneity of such prepared films.

As far as the D and D' peaks is concerned, it is well known that these bands are activated by defects [20, 28, 35, 73, 76]. The onwards challenge is to find a link between these features and the nature of disorder.

Following the guide adopted by several authors, the intensity ratio between D and G peak can be exploited to infer information on the defects [20, 35, 85].

For instance, the most part of the Raman spectra acquired for the GR solutions discussed in this text, have showed I(D)/I(G) ranging from 0.5 up to 1, similar to the values reported by Torrisi and co-workers for sub-micrometric flakes [21]. In the same work, the defect peaks are assigned to flake edges rather than other kind of defects. In addition, because the LPE process is demonstrated not only to determine the separation of the graphite planes but also to affect the flakes lateral size, as a result, the production of platelets with mean lateral size in the order of hundred nanometers is obtained, as confirmed by the DLS measurements and the following TEM images (see next paragraph). Hence, a first indication on the D peak origin due to the flakes edges can be stabilized.

This assignment is further validated by reporting I(D)/I(G) versus FWHM(G) for both NMP (Fig. 3.4a) and H_2O-IPA exfoliated GR (Fig. 3.4b).

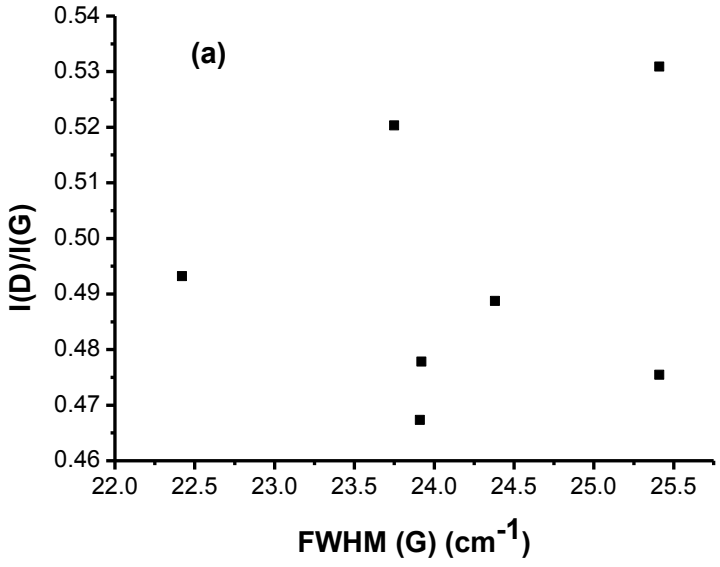

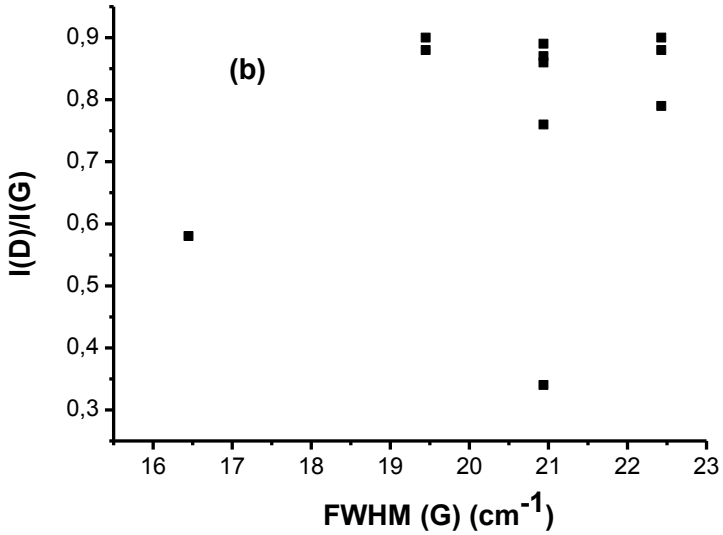

Fig. 3.4: I(D)/I(G) as function of FWHM(G) for (a) NMP and (b) H2O-IPA exfoliated graphene. In both cases, the absence of an evident correlation between the two parameters is highlighted.

Analogously to what reported in Ref. [21], the lack of a correlation in both data set is visible at first sight. In that paper, the authors claimed that the intensity ratio I(D)/I(G) with FWHM(G) allows to discriminate between disorder localized at the edges and disorder in the bulk of the samples. Because a higher I(D)/I(G) would correspond to higher FWHM(G) for bulk disorder, if no relationship is found thisclearly suggests that the major contribution to the D peak comes from the disorder localized at the edges.

Another powerful tool used to discriminate between sp^3-defects, vacancy-like defects and boundaries has been developed by the Casiraghi's group who exploits the intensity ratio between D and D' peak [28]. Although D′ is not much studied in the literature because of its relatively small intensity compared to the D peak, they proved that I(D)/I(D′) is roughly equal to 13 for defects associated with sp^3-hybridization, decreases till to ≃7 for vacancy-like defects and reaches the minimum value (≃3.5) for boundary-like defects for GR flakes produced by anodic bonding and mechanical exfoliation.

In the GR films herein presented, I(D)/I(D′) values up to 2.5 have been calculated. The disagreement with the paper can be easily explained by considering both the different GR production methods with respect to LPE used herein and the concentration of defects. The ratio values reported there, in fact, were obtained in

the approximation of low defects concentration. Taking into account these differences,

1. defects due to the sp^3 bonds and related to basal plane can be definitively discarded since in such a case the ratio should be much more higher than 2.5;

2. on the contrary, $I(D)/I(D') \simeq 2.5$ can be compared with that reported in Ref. [28].

Further evidence of the integrity of the basal plane for chemically exfoliated graphene is provided by Coleman and co-workers [44]. In the cited paper, they found that the flake dimensions of graphene exfoliated in NMP, undergone to sonication and centrifugation process, scale as $t^{1/2}$, t being the sonication time, and that the sonication process is responsible for the defects formation. From the dependence of I(D)/I(G) ratio on the sonication time they inferred the observed defects are likely associated with the edges and the bodies of the flakes are relatively defect free.

Therefore, the boundary–like nature for LPE defects can be assumed. As such, also the approximation of low defects concentration supposed in the aforementioned paper can be discarded in the case herein presented since the LPE GR films are built up by patchworks of sub-micrometric flakes in which edges play a key role, as discussed in the next paragraph.

3.2.1 Transmission Electron and Atomic Force Microscopy characterizations

Transmission Electron Microscopy (TEM) and Atomic Force Microscopy (AFM) are discussed in this section as applied to LPE GR with the purpose to extract other morphological and structural information regarding the exfoliated material.

TEM images have been taken by means of FEI TECNAI G12 Spirit-Twin operating at 120 kV. The samples have been prepared by dipping Cu standard holey carbon grids (400 mesh) into the colloidal suspensions.

Analogously to the Raman characterization, AFM images have been collected from GR films deposited onto the Si/SiO_2 substrate, using the Ntegra Spectra microscope in semicontact mode.

Examples of TEM and AFM images for both examined suspensions are reported in Fig. 3.5, where groups (a) and (b) refer to NMP and H_2O-IPA exfoliated GR, respectively. Noteworthy, due to the substantial homogeneity of the suspensions, demonstrated in the previous paragraph, these images can be estimated as representative of the overall samples.

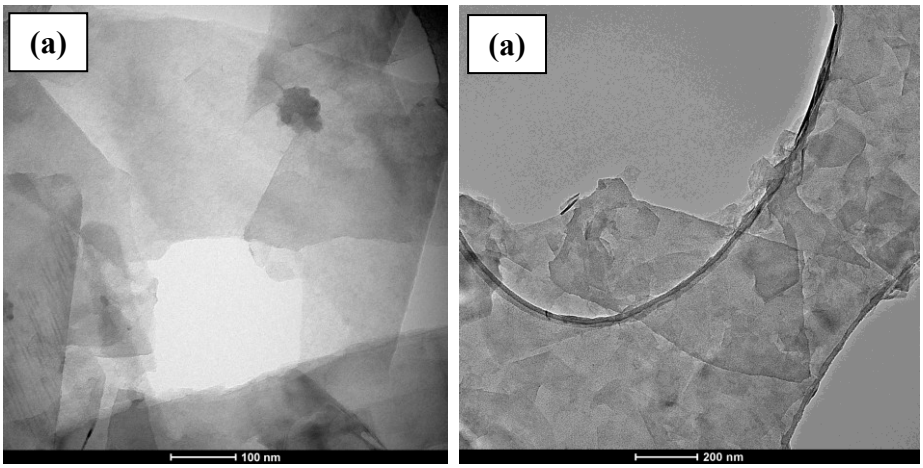

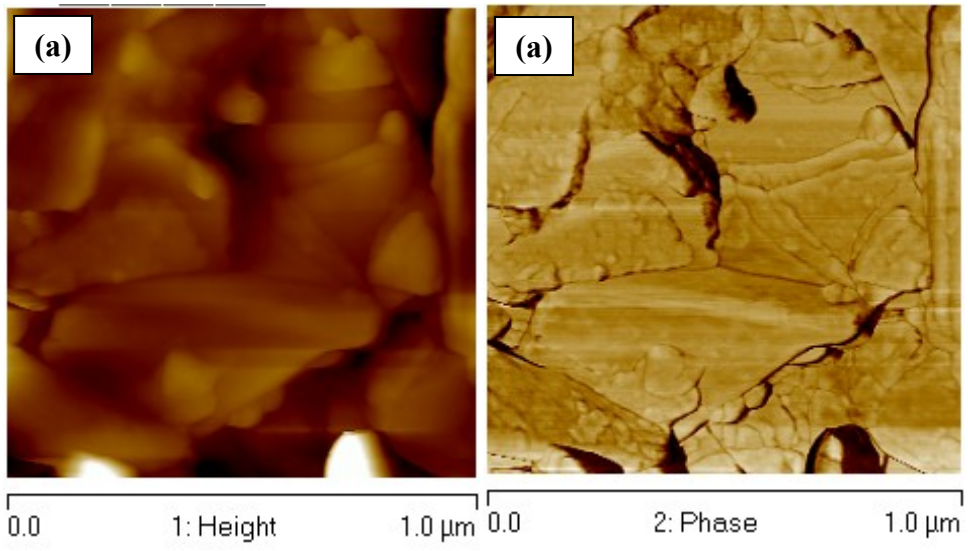
(a)
(a)
0.0
1: Height
1.0 µm
0.0
2: Phase
1.0 µm

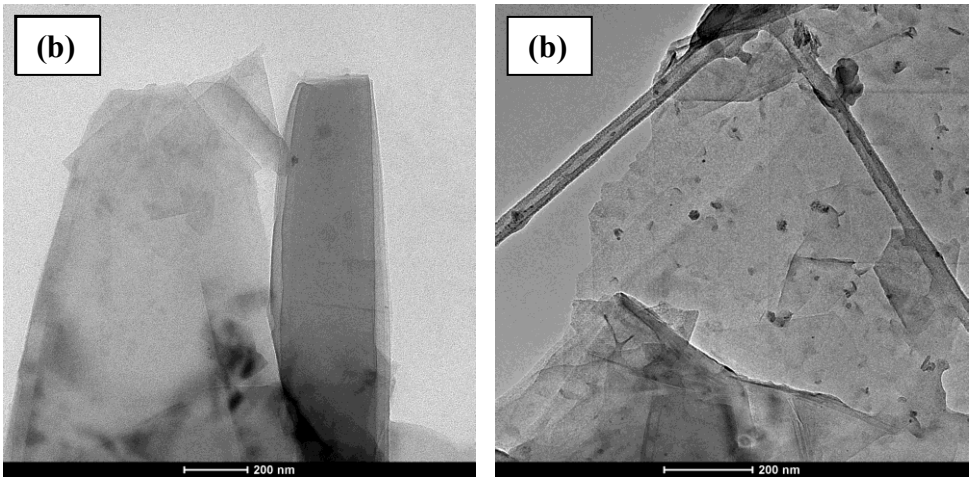
(b)
(b)
200 nm
200 nm

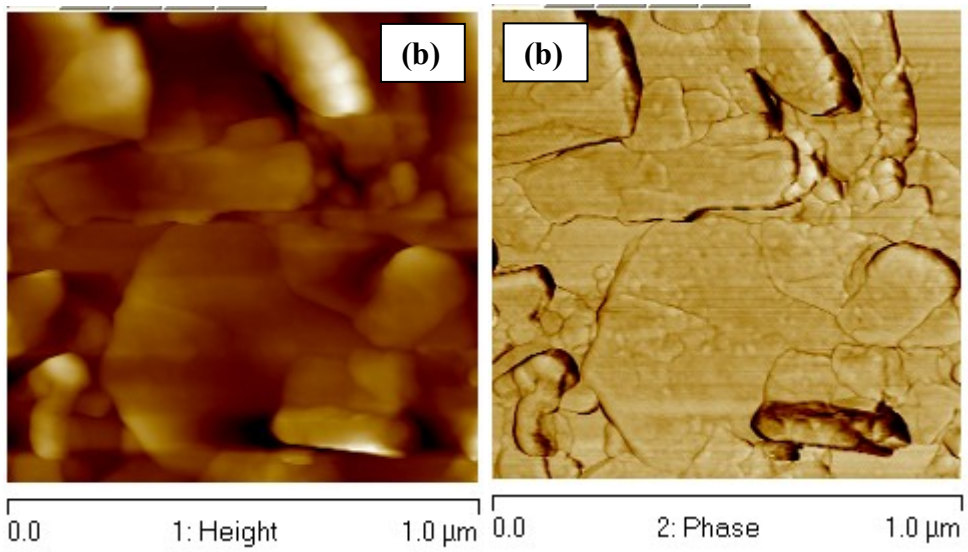
(b)
(b)
0.0
1: Height
1.0 µm
0.0
2: Phase
1.0 µm

Fig. 3.5: TEM and AFM images of (a) NMP and (b) H_2O-IPA exfoliated graphene. The scale bars confirm the flakes mean size in the range of few hundred nanometers. For the AFM images, the profile (on the left) and the phase (on the right) are reported.

Both groups of images in Fig. 3.5 permit to demonstrate what has been previously stated. Firstly, starting from the TEM images, the high degree of graphite exfoliation for both suspensions is confirmed, disclosing FLG, SLG and sparse thicker fragments arranged in a nearly continuous film either way. Then, the scale bars show that the flakes mean lateral size in the range of few hundred nanometers is achieved.

Examining the AFM pictures, besides on the confirmation of the flakes dimensions, that can be easier inferred from the phase image, a further analogy between the two solutions is found. The roughness value, in fact, results to be roughly 24 nm and 18 nm for NMP and H_2O-IPA exfoliated GR, respectively. Taking into account the tendency to wrap of the LPE GR films onto the substrate and, in turn, the difficulty to estimate this parameter, the two values can be fairly comparable.

Finally, as regards the defects issue, both characterizations in either cases testify the quite huge amount of edges in the films. Therefore, the boundary-like nature of defects, introduced with the Raman discussion, can be definitely confirmed. Additional proofs will be given in the following, discussing GR grown by CVD.

In summary, because defected GR has been demonstrated to be more reactive towards molecules (see Chapter 2), the sub-micrometric dimensions of the flakes and, in turn, the presence of edges allow to easily understand why this kind of material is particularly suitable in the gas sensing field, as it will be demonstrated in the next chapter.

3.3 Chemical Vapor Deposition: the procedure

The overall CVD procedure consists of different steps, especially for what concerns the transfer process from the catalyst to the target substrate. Indeed, with the aim to obtain a film as much continuous and clean as possible , several parameters in the transfer need to be adjusted. Hence, in the following, firstly the optimized procedure is reported, then the most significant employed attempts and related characterizations to arrive at the complete procedure are presented.

Fig. 3.7 displays the temperature profile of the process cycle for GR growth on Cu by CVD, performed using an AIXTRON Black Magic Pro system at 25 mbar.

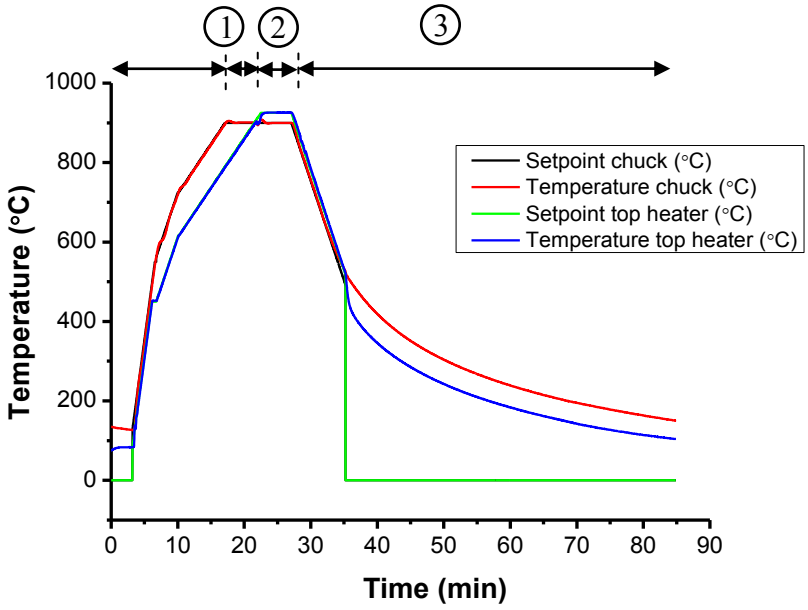

Fig. 3.6: process cycle of graphene growth on Cu displaying the temperature profile. The curves are referred to the set and read temperatures in the reactor: black and green lines report the set points on the chuck and top heater, respectively, while red and blue lines show, respectively, the read temperatures by the thermocouple put on the chuck and by the sensor placed on the top heater.

Due to the thermal inertia determining a small difference between the set point and the actual temperature value, in Fig. 3.6 four curves are reported: black and green lines are referred to the set points on the chuck and top heater of the reactor, respectively, whereas red and blue lines show, respectively, the temperatures read by the thermocouple put on the chuck and by the sensor placed on the top heater.

During the first 18 min, the Si wafer with Cu[5] is brought gradually[6] to 900 °C in Ar and H_2 atmosphere and then annealed for about 5 min in order to remove the native oxide (step 1 in Fig. 3.6). Subsequently, CH_4 is introduced in the chamber for about 5 min (step 2 in Fig. 3.6) and finally the chuck is cooled down from 900°C to 500°C (step 3 in Fig. 3.6) with a rate of 50°C/min in order to reduce stress in the film.

The cooling is the most critical phase in the growth process since, during this step, damages can be easily generated in the film. A gradual cooling rate reduces stress and cracks in the film.

The growth is followed by the critical and tricky transfer phase from the Cu to the target substrate, that is SiO_2/Si (see Chapter 2). The optimized procedure herein described is a combination between the two methods discussed in the previous section (Par. 2.1.1) and the specific steps can be set as follows.

1. The wafer (GR/Cu/SiO_2/Si) is mildy treated for 10 min in Hexamethyldisiloxane (HMDS) bath to favor the PMMA adhesion.
2. PMMA dissolved in chlorobenzene with a concentration of 46mg/ml is spin-coated at a speed of 1500 rpm for 60 s (acceleration of 1000 rpm/s). The resulting PMMA thickness is approximately 2 μm.
3. A soft baking is required to cure the PMMA: 150°C for 60 s on hotplate.
4. After the baking process, the sandwich (PMMA/GR/Cu/SiO_2/Si) is cut into pieces of about 1cm^2. The samples area need to be a trade-off between two requirements: the etching time of the catalyst (discussed below) and the way to handle the samples.
5. Sticky gel-pak elastic sheet (GP) is placed on the sandwich and is gently pressed to make sure that GP and P MMA have a good contact.
6. The GP/PMMA/GR/Cu/SiO_2/Si samples are put into a $FeCl_3$+H_2O solution at 8% using a Teflon colander. When the Cu foil is etched away from the Si substrate, the Si piece falls down in the colander while the GP/PMMA/GR stack floats on the solution. The duration time of this step strictly depends on the sample size and the dilution of the etching solution.

[5] A thin film of Cu (500 nm) is deposited through magnetron sputtering at room temperature with pure Cu (99.995%) target on Si (100) wafers coated with 100 nm thermal oxide.
[6] Some attempts of growth have been performed at T=925°C, however being this point quite closer to the Cu melting point (1085°C) pinholes have been observed onto the films.

7. The GP/PMMA/GR stack is then gently cleaned with water, in order to remove the residues of the etching solution, and kept in air for almost 2 hours with the GR face up, in order to dry the stamp before transferring on the target substrate.
8. The dried GP/PMMA/GR stack is placed on a wafer (SiO_2/Si) with the GR layer facing down. This whole system is baked on a hotplate set at 160°C for 10 min with gentle pressure on GP.
9. Operating on the hotplate, the GP sheet is slowly peeled off and the PMMA/GR film keeps attached to the target substrate.
10. The colander with PMMA/GR/ SiO_2/Si sample is rinsed, firstly, in NMP for 8 min at 70°C to remove PMMA, then in IPA for 3 min and finally in water.

The step by step optimization of this recipe has been driven basically by three requirements: 1. the preservation of the GR film integrity and cleanness; 2. the achievement of the largest possible flakes dimension; 3. the completion of the overall process in the shortest time possible.

With the above-mentioned points in mind, the following flow chart resumes some parameters and attempts performed for the recipe optimization, especially for what concerns the point 1.

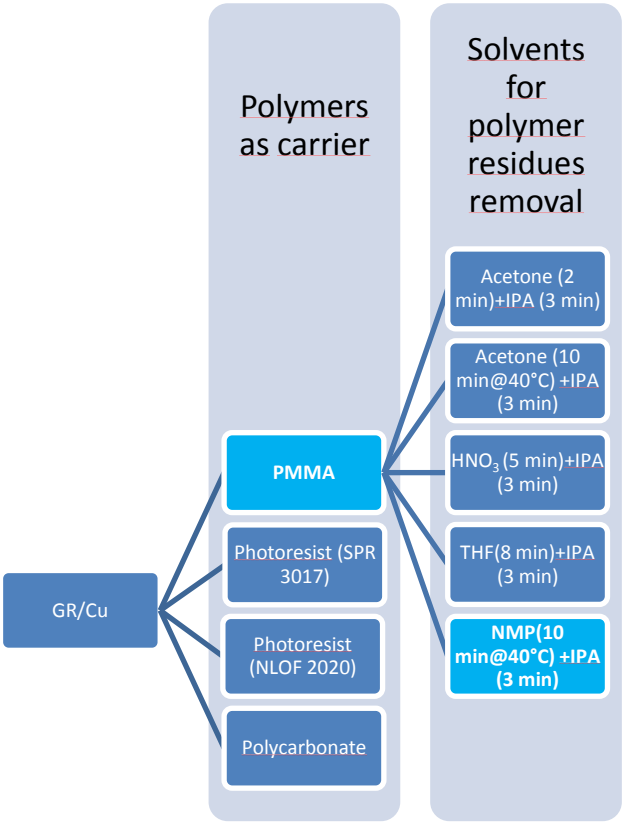

Fig. 3.7: parameters taken into account for the recipe optimization. The lighter rectangles indicate the final choice.

As carrier film, PMMA is the polymer allowing to reduce the GR cracks and to obtain the larger and cleaner flakes with respect to the other polymers. However, PMMA residues are confirmed to be not easily removable at the end of the process [95], that is why several solvents and combinations have been tested. Noteworthy, impurities and defects can be introduced during the transfer process, resulting in a rise of improper peaks in the Raman spectrum, as it will showed later. Therefore, in order to exactly address the nature of peaks and bands, it is essential to reduce the presence of unknown prominences.

As far as the latter requirement is concerned, for instance, in Fig. 3.8 the employed attempts for the Cu etching time as function of $FeCl_3$+H_2O solution are reported.

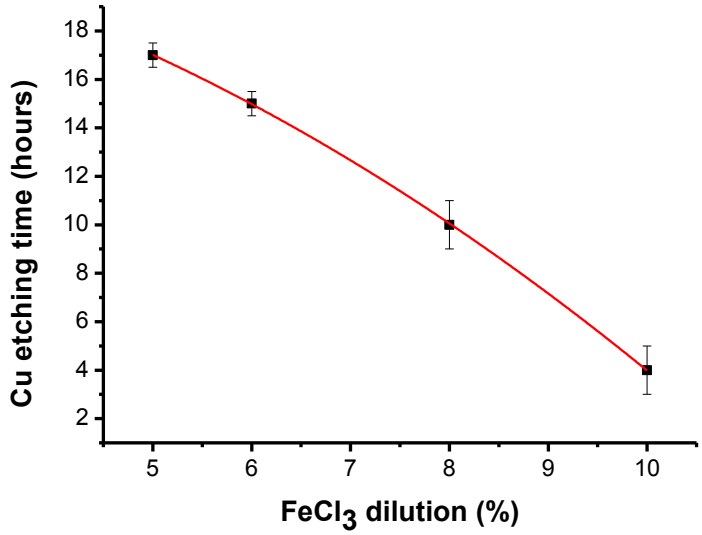

Fig. 3.8: Cu etching time as function of $FeCl_3$ dilution for GR samples with area approximately 1 cm^2.

The fitting curve (red line) in Fig. 3.8 not only shows a fairly match with the experimental data but also provides a calibration plot for further attempts.

3.4 Characterization of CVD graphene

In Fig. 3.9, the Raman spectra of CVD grown GR are presented. In order to be sure of the GR growth, the lower four spectra have been taken directly on the catalyst substrate (Cu) in the same set up conditions previously described; the upper four spectra have been captured on the target substrate. As a matter of fact, both groups come from the average on five values collected in different points of the film on Cu and SiO_2/Si, respectively. All spectra are normalized to the 2D band intensity

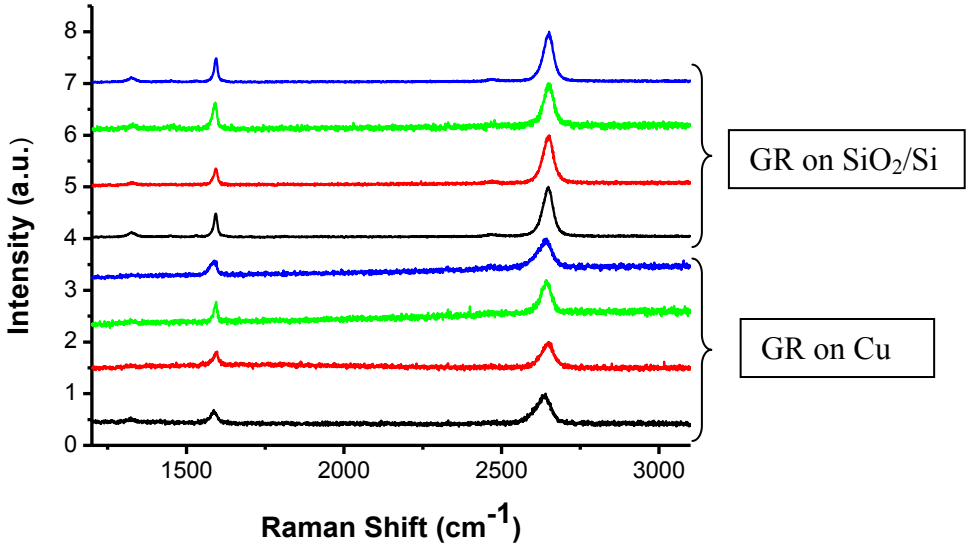

Fig. 3.9: typical Raman profiles for CVD grown GR captured on the copper (first four spectra at the bottom) and on the target substrate (other spectra), respectively.

With respect to the spectra captured on the SiO_2/Si, the first group of spectra present a higher noise due to resonances of the Cu activated by the laser. However, apart this difference the typical profiles of CVD grown GR can be easily recognized on both substrates. To this regard, a deep investigation is presented in the following.

For instance, in Fig. 3.10, the spectrum of graphite (black line), CVD grown GR (red line) and ME GR[7] (green line) are reported, being the latter two films deposited on SiO_2/Si. Also for this group, all spectra are normalized to the 2D band intensity. In the inset, a picture of CVD grown GR film taken under the optical microscope is showed.

[7] These flakes as well the production technique were presented and discussed in my master thesis [37].

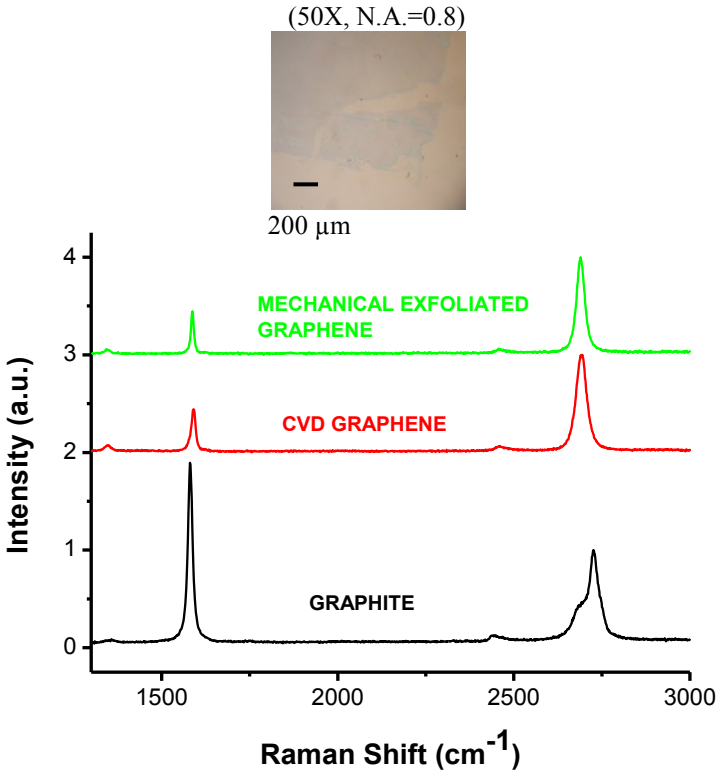

Fig. 3.10: Raman spectra for CVD grown GR (red line) and in ME GR (green line); as comparison, the black line shows the graphite spectrum. The intensities are normalized to the 2D band. Inset: optical image of CVD grown GR film on SiO_2/Si.

Aclear evolution can be observed in the passage from graphite to GR. Firstly, there is the inversion of the relative ratio between I(G) and I(2D); then the two components of the graphite 2D band presented in the previous paragraph become only one peak, that can be fitted with a single sharp Lorentzian (see Fig. 3.11) [76].

Also the comparison between ME and CVD is remarkable interesting. The two profiles, both referred to SLG, are perfectly comparable, suggesting that the material quality of ME GR has been finally achieved, as it has been stated in Fig. 2.2. The only handicap with respect to ME is the laboriousness affecting the CVD recipe, as described in the previous paragraph. However, this is the only ticket to pay on the road of the large scale production.

By focusing on the 2D band, in Fig. 3.11 an explosion of the spectra peaks reported in Fig. 3.10 is exhibited.

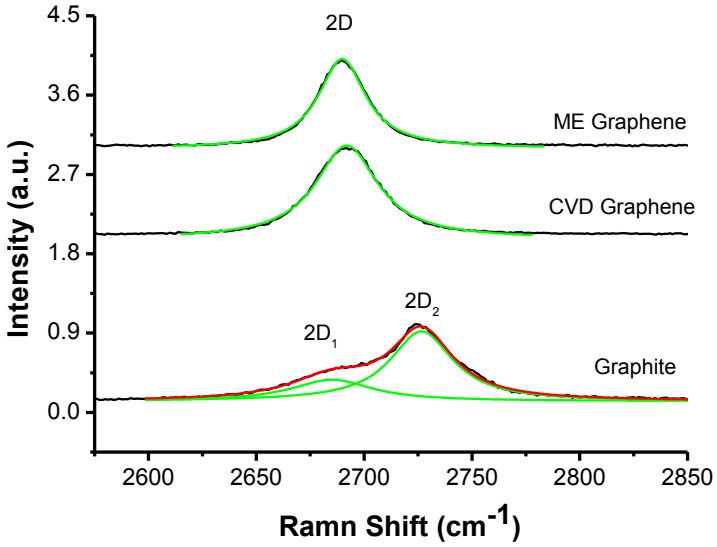

Fig. 3.11: Zoom on the 2D band of graphite (lower spectrum), CVD GR (middle spectrum) and ME GR (upper spectrum). All spectra are normalized to the 2D intensity. The deconvolution and the fit of the 2D band are reported as green line, whereas the black line reports the profiles and the red one in the lower spectrum is the sum of the two components.

The Lorentzian curves (green lines) fitting the 2D peaks of CVD and ME GR have FWHM roughly 34 cm^{-1} and 26 cm^{-1}, respectively. If compared with the value usually reported in the literature for SLG (~25 cm^{-1}) [76], this firstly means that the exact way to produce SLG has been definitively found. In addition, the outstanding findings further allow to demonstrate the equivalence between CVD and ME technique.

As regards the D peak usually rising at ~1350 cm^{-1}, the Raman spectra herein presented are almost totally D-peak free.

The lack of D peak in such prepared CVD GR allows to put a significant contribution in understanding the defects issue for LPE GR, as discussed later.

Fig. 3.12 shows two AFM images of CVD GR transferred on SiO_2/Si substrate. Due to the homogeneity of the GR film that has been demonstrated by the Raman characterization, the images can be considered representative of the whole sample. The same operating set up conditions described for LPE GR characterization have been adopted.

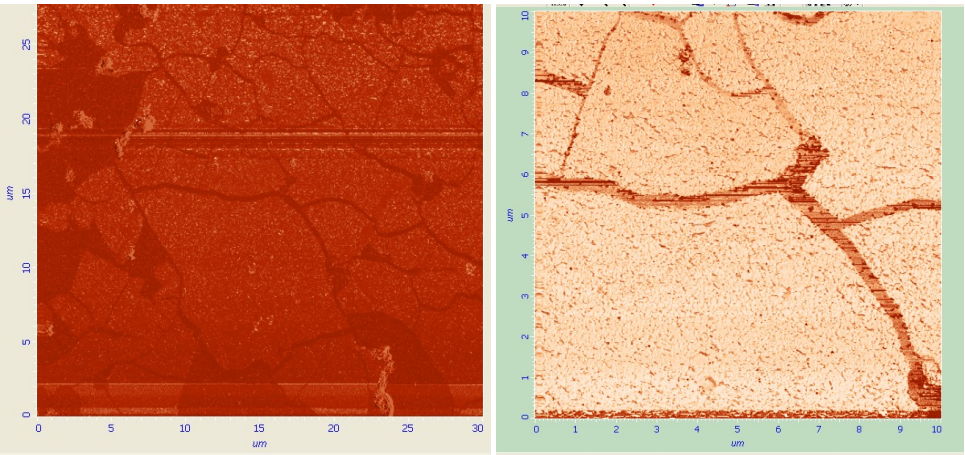

Fig. 3.12: AFM images of CVD GR depositated on SiO_2/Si. Flat and smoth flakes with lateral size in the range of few ten micrometers are visible.

The images exhibit extremely flat and smooth flakes with mean lateral size approximately 10-20 μm. Maximum size up to few millimeters can be sometimes achieved (e.g. see the optical image in Fig. 3.10). On the other hand, in Fig. 3.12 wrinkles appear on the films, likely due to the gentle pressure applied during the step n. 8 of the transfer procedure (Par. 3.3). A further improvement of this step will pave the route to produce larger and much more continuous films. However, the achieved result in flake dimensions indicates that CVD flakes are several orders of magnitude bigger than the LPE ones. In turn, taking ideally into account the same area of the GR film, the edges density results to be completely incomparable between the materials prepared by the two techniques.

This crucial difference definitely allows to understand the edges nature for LPE GR. At the same time, the edge defects can be assumed as the major players for the better performances of LPE GR-based chemi-resistors with respect to those based on CVD GR, as it will be discussed in the next Chapter.

3.5 Conclusions

In this Chapter, GR prepared by LPE and CVD has been reported and widely investigated through several characterization techniques, including Raman spectroscopy, AFM and TEM.

The Raman analysis has allowed to infer that LPE material is composed by flakes with number of layers equal or less than five. The Raman spectra has also provided information on the presence of some defects that TEM and AFM have confirmed to be due to the edges of flakes. Furthermore, TEM and DLS results have pointed out that the nanoplatelets have mean lateral size in the range of hundred nanometers and result to are arranged in a nearly continuous film. By means of these characterization techniques also the perfect equivalence between the two GR suspensions has been demonstrated. The first one, totally ideated and realized by ourselves, has been prepared by exfoliating graphite in a green solvent, i.e. H_2O-IPA; the second suspension has been realized using NMP as solvent.

As regards the CVD technique, the recipe for growth of GR has been presented. Also all steps of the optimized transfer procedure have been described, mentioning all parameters taken into account for the process optimization. Raman Spectroscopy on CVD GR has permitted to fully characterize the material, demonstrating the successfully achievement of SLG growth on Cu and transfer on SiO_2/Si. The flake sizes are in the range of few ten micrometers, as it has been confirmed by AFM measurements. By comparing CVD GR with ME one presented in my master thesis, the extremely high quality of the former one has been demonstrated.

Finally, by cross-checking the obtained results for LPE and CVD GR, the nature of defects has been definitively disclosed, especially for LPE GR: defects are not due to crystalline imperfections but only to the flake edges. This assessment also permits to clearly explain the different behavior of the chemi-resistors based on LPE and CVD GR, that will be discussed in the following.

CHAPTER IV

GRAPHENE-BASED CHEMI-RESISTORS FOR NO_2 DETECTION

This Chapter illustrates the behavior of a chemi-resistor based on LPE GR detecting NO_2 and operating at room temperature and pressure as well as in presence of humidity. In the first part of the section, the questions related to the devices preparation by drop-casting and the differences from device-to-device performances are investigated. Starting from the absence or slow recovery after the signal output of the chemi-sensor, a new approach to overcome this bottleneck is introduced. This method, besides providing a solution to the recovery problem, allows calibrating the sensor in a large range of concentrations from 100 ppb up to 1000 ppb, making the device particularly appealing as graphene-based sensor for NO_2 operating in wet environment. Finally, the chemi-sensor based on CVD grown GR is introduced and the performances in NO_2 detection are compared with those related to the first discussed device.

4.1 Notes on devices preparation and experimental set up

The chemi-resistor is the simplest conceivable transducer structure to be used as chemical sensor, since the interaction between the active medium and the analyte determines a resistance change. Accordingly, the current variations represent the output in response to the gas inlet.

The LPE GR-based devices presented herein are prevalently prepared by drop casting, a simple technique that does not require laborious equipment. In our case, it consists in depositing a fixed GR suspension volume onto alumina (Al_2O_3) substrate[8] on which interdigitated gold electrodes (IDE) are printed (Fig. 4.1). The transducers are finally heated at 130-150°C to promote the evaporation of solvent residues that may persist in the deposited film.

[8] The detailed information regarding the transducer are reported in Appendix A.

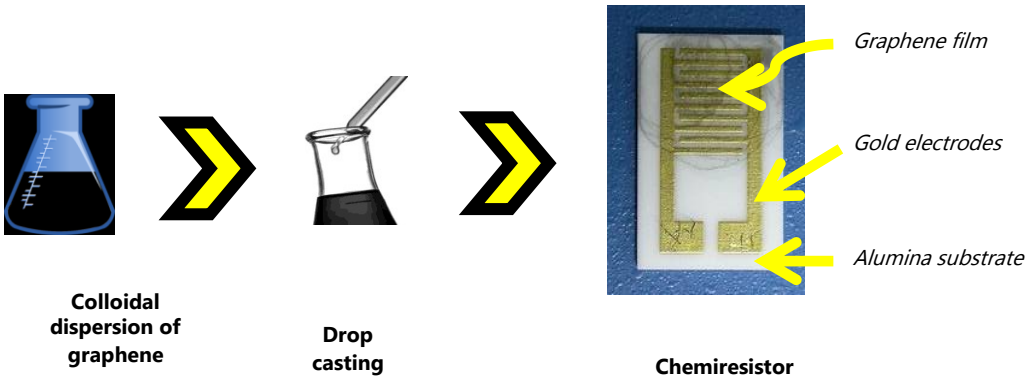

Fig. 4.1: flow chart for the chemi-resistor preparation by drop casting of graphene suspension

In spite of the same suspension volume is deposited on the transducers and although the technique is fairly easy to be used, the drop casting is affected by the lack of uniformity since the drops can spread randomly onto the transducers. This means that variations of the initial device resistance and differences from device-to-device performances in detection could be obtained (see next paragraph). Indeed, two different routes have been thought to run:

1. the development of an approach able to correlate the analyte concentrations with the conductance variations of the device, independently of its original properties, as deeply discussed later;
2. a different deposition technique, such as the ink-jet printing, has been starting to investigate since it can provide a better control on the dispersion homogeneity [96].

Generally, to have first indications and evaluate the device performances in sensing measurement, a standard protocol is adopted, which basically consists of three steps (refer to Fig. 4.2):

- a baseline in which only a carrier gas is flowed, typically synthetic air or nitrogen. This step serves both to stabilize the device in the environment in which it is enclosed and to determine the starting point of the sensor response at the gas inlet;
- a time window during which the analyte in an appropriate concentration is flowed;
- a final step, namely the recovery, in which only carrier gas is again present and it is needed to restore the device at the initial conditions.

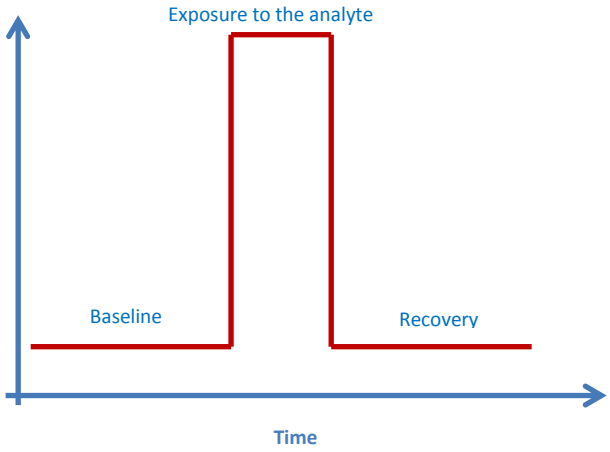

Fig. 4.2: sketch of standard protocol for sensing measurement representing the three steps as function of time: 1. the baseline; 2. the gas exposure; 3. the recovery. The y-axis is dimensionless since the physical quantity to be monitored depends on the transduction mechanism.

The described protocol, besides being the simplest test performed on gas sensitive devices, is aimed to simulate a real event that can happen in common life and represents the ideal sensor behavior when it is exposed to a gas flow[9].

In Fig. 4.2, the y-axis is dimensionless since the physical quantity recorded as function of time towards the gas exposure depends on the transduction mechanism. Because in this section the analyzed sensors are chemi-resistors, the output is the current or, equivalently, the conductance.

Hence, the experimental set up for sensing measurement is a system (Gas Sensor Characterization System, GSCS) equipped to perform volt-amperometric measurements on chemi-resistive devices. Owing to deal with sensors operating in environmental conditions, the most important requirement of ENEA GSCS[10] is the exact reproduction of these conditions in terms of room temperature and pressure as well as relative humidity (RH)[11].

[9] The described protocol can be generally applied to all sensors put through an external perturbation. In this case, the baseline and the recovery represent the status of the device immediately before and soon after the perturbation, respectively.
[10] The equipment detailed description is reported in Appendix B.
[11] The relative humidity (RH) is defined as the ratio between the amount of water vapor contained in the air mass and the maximum amount of water vapor that the air mass can contain in the same conditions of temperature and pressure (saturation). That is why RH is expressed as percentage.

4.1.1 Differences from device-to-device performances

In Fig. 4.3, two examples of GR-based chemi-resistor[12] behavior upon the previously described protocol are showed.

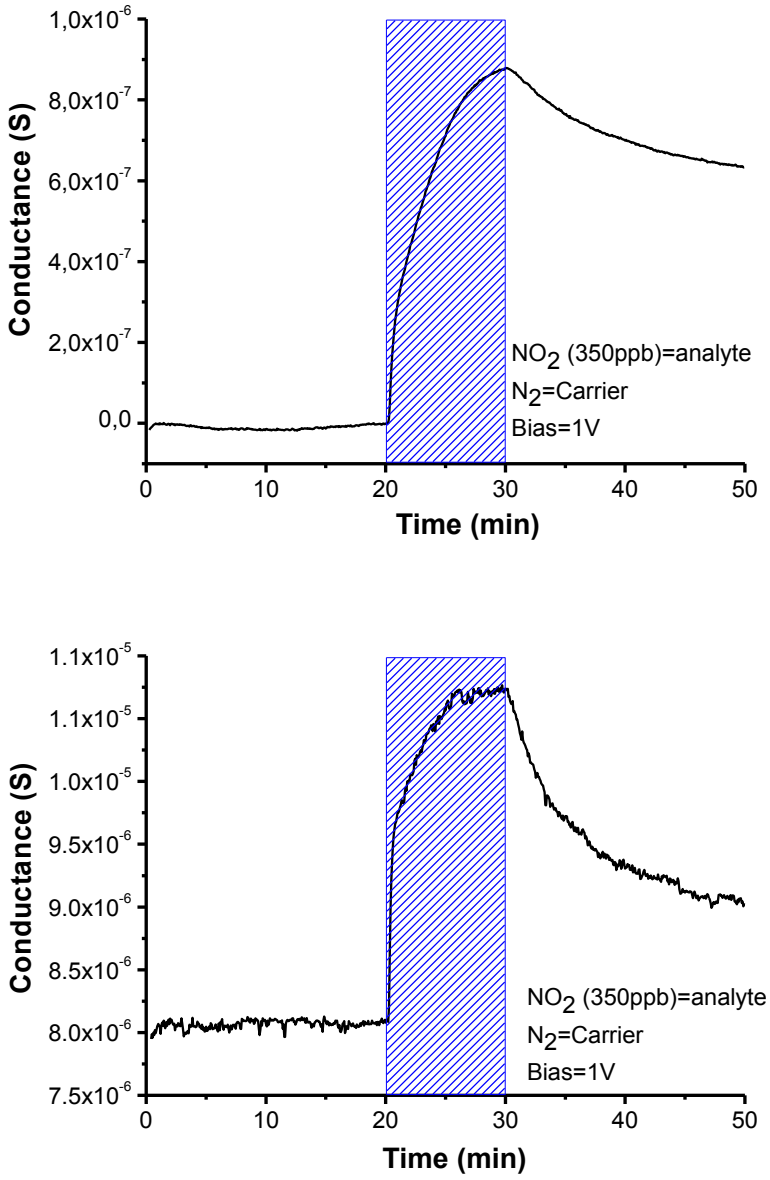

Fig. 4.3: two examples of GR-based chemi-resistor dynamic response towards 350 ppb of NO_2. The dashed blue area represents the exposure window towards the target gas.

In particular, the employed test, called **Test1**, is set as follows:

- 20 minutes in N_2 as carrier gas;

[12] After drop-casting GR suspension on IDE, a volt-amperometric characterization is performed for each prepared device in order to verify the effectiveness of the contacts realization and the ohmic nature of the GR/Au junction.

- 10 minutes exposure to 350 ppb of NO_2;
- 20 minutes of flushing with N_2.

RH and temperature are set at constant values of 50% and 22°C, respectively.

Although Fig. 4.3 shows behaviors quite different from that reported in Fig. 4.2, the efforts are addressed to make sensors as much similar as possible to the ideal one. On the other hand, these two preliminary tests allow to highlight some fundamental features:

1. the GR-based chemi-resistor exhibits a current increase during the exposure time. Because NO_2 is a well known oxidizer, the observed increase in the current is therefore naturally expected as a result of molecule interaction with a p-type material if, during the interaction, an electron can be partially transferred from the GR to the analyte. The p-type main carrier behavior has been confirmed by Seebeck effect evaluation [4, 37, 71].

2. a remarkable signal variation towards only 350 ppb of NO_2 can be observed. In other words, we obtain signs that chemi-resistors based on LPE GR and operating at RT can be able to detect such low analyte concentration so that they could represent the ideal candidate to be adopted in real atmosphere;

3. the signal does not present saturation during the exposure. The main reason for this behavior is that the GR film is composed by a patchwork of sub-micrometer flakes that provides an extremely high number of sites available to the interaction with the analyte. In addition, also the presence of boundary like defects is notably huge, offering further reactive sites to the interaction with the molecules and contributing to hardly reach the complete occupation of all sites and, in turn, the signal saturation;

4. expanding the output around the instant in which gas enters into the chamber, e.g. 20 minutes from the test start, it could be observed an immediate increase of the current signal, testifying the extremely high response readiness of the device towards toxic gas.

5. after the exposure to the target gas, either way the signal is not able to return at the value assumed at the gas inlet. This point will be better discussed in paragraph 4.1.2.

Fig. 4.3 allows also to outline the item related to GR chemi-resistor performances and reproducibility that seem to be strongly dependent on device

fabrication, including film deposition. In our previous work, in fact, we have proved that, even though GR materials come from the same batch and the same fabrication protocol, as happens for devices considered for measurements in Fig. 4.3, the results can vary from one to another (Table 4.1) [8]. The device parameters taken into account in Table 4.1, i.e. resistance, conductance variation and SNR, are defined as follows:

- resistance is the value measured soon after the device preparation;
- the conductance variation was calculated as $\Delta G/G_0$, where G_0 represents the conductance value soon before the introduction of the analyte, referring to the test measurement shown in Fig. 4.3;
- SNR was evaluated as $SNR=G_{max}/A_{noise}$, where G_{max} represents the maximum conductance value during the exposure time and is the maximum amplitude of the noise oscillation before the analyte inlet [89].

Name	*Resistance (kΩ)*	*Solvent*	*Centrifugation speed (rpm)*	*Centrifugation time (min)*	*Conductance variation (%)*	*SNR*
DEVICE 1	50000	NMP	500	45	1,3	42
DEVICE 2	180	NMP	500	45	0,9	199
DEVICE 3	460	NMP	500	45	7,7	42
DEVICE 4	5,14	NMP	500	90	5,6	1656
DEVICE 5	73,7	NMP	500	90	1,9	134
DEVICE 6	8,5	NMP	2500	90	0,6	1646
DEVICE 7	4,2	NMP	2500	90	1,2	128
DEVICE 8	44,6	NMP	13000	90	2,2	1150
DEVICE 9	4,14	NMP	13000	90	4,1	1012
DEVICE 10	173	DMF	13000	10	3	197
DEVICE 11	400	DMF	13000	10	11,7	226
DEVICE 12	16,6	DMF	13000	10	3,2	510

Table 4.1: recipes utilized for the material preparation and results obtained by applying Test1 to several chemi-resistors towards 350 ppb of NO_2.

For example, looking at the first three or the last three devices, in principle they are thought to be equivalent, having GR materials coming from the same batch and being the devices fabricated with identical procedure, but the respective values in the first column or in the last two ones testify remarkable differences in their performances. These can be explained by considering the lack of homogeneity in the dispersion deposition by drop casting: the different contact between GR and IDE can affect both the resistance value and the presence of different paths for the

charge carriers. As a result, the signal or noise can improve or become worse and different SNR values are determined [8].

As such, these findings, jointed to the difficulty to reach a complete recovery for sensors operating at RT (see Chapter 1 and next paragraph), aim to uncover how strong efforts need to be done in order to enhance the effective devices reproducibility.

4.1.2 A simple method to recover the graphene-based chemi-resistor signal

By analyzing the diagrams in Fig. 4.3, the other device feature catching immediately eyes regards the recovery step.

It is well known that a crucial point for solid-state gas sensor use at RT is the difficulty to return at the initial conditions after the sensing operation. The drawback arises from the interaction energy between sensitive materials and gases, as reported by conventional transition state theory. At RT, in fact, the energies involved in the adsorption phenomena are in the range of eV, so that, once chemisorbed, reversibility is not thermodynamically favored [97]; at high temperature, instead, the adsorbates desorption is better allowed, which is why MOX-based sensors, for example, work better in this scenario than at RT (see Chapter 1). Because the absence of recovery makes the device useless or, better, allows to use it just one time, this issue has been deeply investigated in our previous work [98].

We considered two GR-based chemi-resistors, differing each other for the feed recipe preparation: in one case, GR suspension was prepared dispersing graphite flakes (Sigma-Aldrich, product N.332461) at 2.5 g/l in NMP, in the other case a mixture of isopropanol and n-butanol (IPA/n-BuOH) replaced NMP as solvent[13]. Then, in both cases the mild sonication treatment for 168h at low power and the centrifugation at 500 rpm were carried out [44, 98]. The chemi-resistor devices were fabricated by drop casting few microliters of the colloidal dispersions directly onto the alumina substrates and then were tested upon Test1 at three different steps: as soon as prepared, after about one month, during which they were intentionally exposed in air, and finally after applying two restoring methods, namely, the device annealing at 130°C in vacuum for 120 min and a newly developed method which encompasses the dipping of exhaust devices into ultrapure water at 100°C for 60 sec followed by a drying step on the hot plate at 150°C for 5 min. The latter proposed method stems from the strong solubility of NO_2 in H_2O, this dissolution mechanism being well known in the literature [18].

In Fig. 4.4, the stacked curves refer to tests carried out at different times on devices prepared with GR exfoliated in NMP (panel a) and in IPA/n-BuOH (panel

[13] Two recipes have been taken into account with the aim to verify the approach effectiveness on material prepared according to different ways.

b). Because of the huge device current ranges, as previously discussed, the output was normalized at G_0, that is the initial value during the gas inlet.

In Fig. 4.4b, the conductance after the restoration by the annealing method is not reported due to the overall absence of signal in that measurement, indicating that all GR sensing sites could be occupied by the adsorbates so that the sensing layer is insensitive to additional molecules.

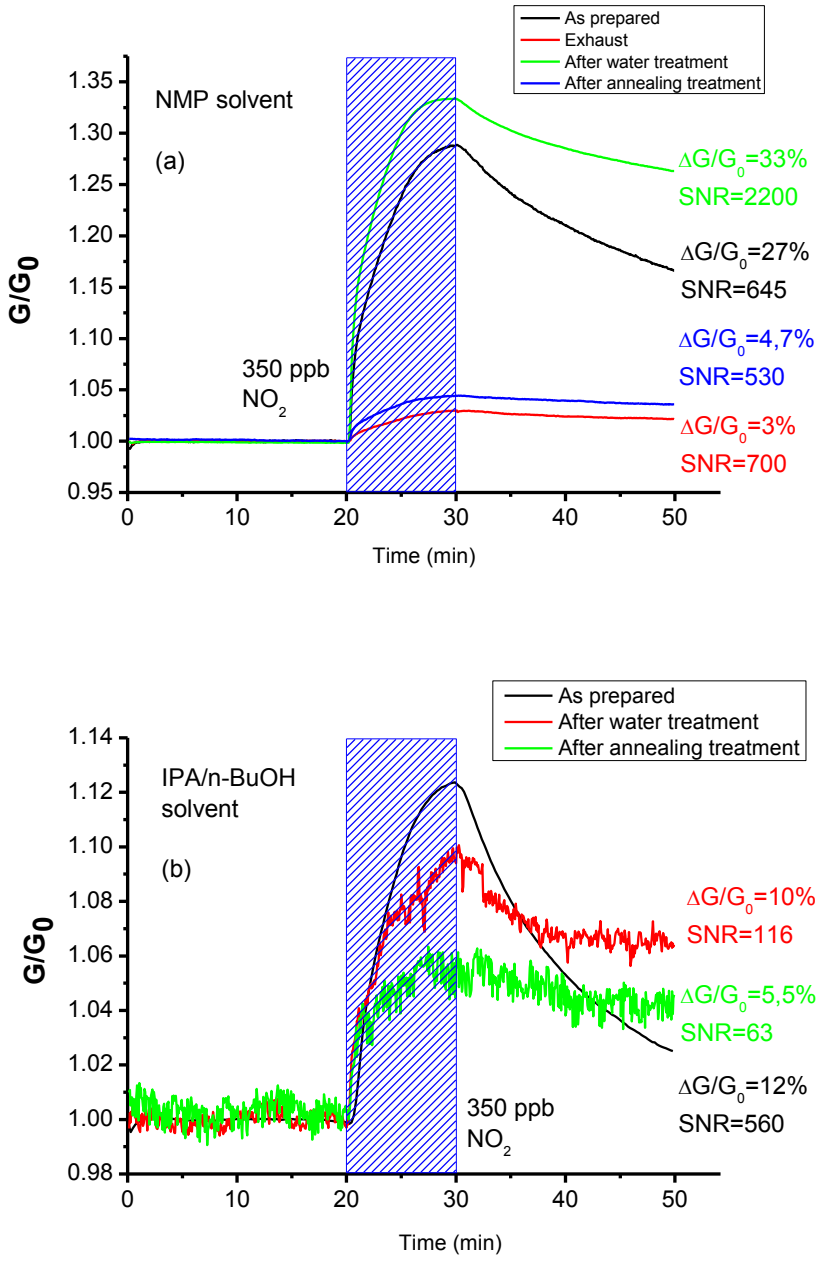

Fig. 4.4: normalized electrical conductance behaviors for chemi-resistors based on GR exfoliated in NMP (panel a) and in a mixture of IPA/n-BuOH solvent (panel b). The described Test1 was applied to devices corresponding to different initial state: as soon as prepared (black line), after the restoration by dipping method (red line), after the restoration by annealing method (green line) and after the restoration by annealing method (blue line). In Panel b, the test after the annealing method is not reported because of the overall absence of signal.

The effects of the refreshing approach on the chemi-resistors can be straightforwardly observed in Fig. 4.4a: the conductance variation after one month (red line) appears almost flat, maybe due to the strong poisoning effect that occurred in storage period by the exposure to contaminants present in the atmosphere, NO_2 included; after the dipping into ultrapure water (green line) the variation becomes about ten times higher (from 3% to 33%), resulting also more intense with respect to the annealing method (black line). The curves in Fig. 4.4b confirm once more that the developed method is able even to restore sensing layers fully insensitive to NO_2 (red line) since the device left in air and then tested again did not give any signal.

Comparing the curves in the panels (Fig. 4.4), a disagreement concerning the SNR values after the restoration by the annealing method is observed. In Panel a, the green curve shows SNR dramatically higher than that referred to response of the as prepared device (2200 vs 645). This does not happen in Panel b, in which the signal after the refresh appears noisier, namely having a lower SNR, than that referred to the freshly prepared device. The main explanation for this phenomenon is that, in the second case, the water treatment could have removed not only the adsorbates from GR surface but also some GR flakes from the alumina substrate, worsening the electrical conduction through the IDE.

The method was applied on other two couples of chemi-resistors, prepared with feed solutions similar to that of the above discussed devices. The reproducibility of the restoration process for the developed approach is confirmed in all four experiments [98].

To summarize, with respect to other more laborious techniques [98], an easy and original method to refresh the exhaust GR-based chemi-resistor after NO_2 exposure has been introduced. This novel approach basically derives from the ability of water to remove the adsorbed NO_2 molecules. The method effectiveness is demonstrated by the fact that devices fully unreactive to the analyte, after the restoration, show performances not only comparable to but in some cases even better than those obtained when the device is freshly prepared.

4.2 A new approach for the sensor response

In most of the common applications, the operating mode for gas sensors requires cyclical exposures to toxic gases. Consequently, equivalent events are obviously expected to return the same output. A way to face up the device reproducibility, has been explored using a GR-based chemi-resistor (inset in Fig. 4.5) with material exfoliated in NMP [4].

To this aim, an appropriate protocol, named **Test2**, has been written out. It represents an up-grade of **Test1** and consists in repeating cyclically for three times the steps involved in **Test1**: baseline (20 min), exposure towards 350 ppb of NO_2 (10 min) and recovery (10 min). In Fig. 4.5, the conductance dynamic response is shown.

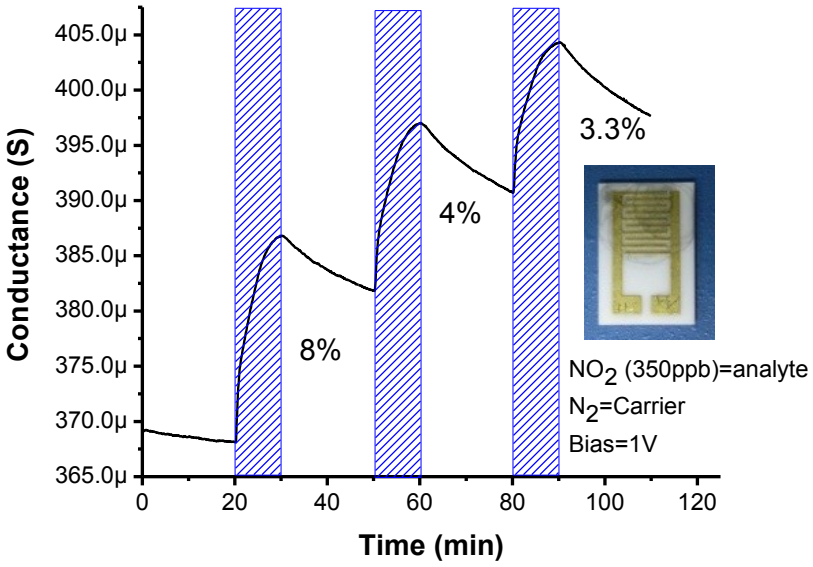

Fig. 4.5: conductance dynamic behavior of GR-based chemi-resistor as response upon protocol named Test2. It consists of three sequential repetitions of Test1 towards 350 ppb of NO_2 (dashed blue areas). Each single exposure to the target gas is characterized by a worsening of the conductance variation, passing from 8% in the first run to 3.3% in the last one, and a partial, slow recovery to the initial conditions. Inset: picture of tested GR-based chemi-resistor.

Focusing on the single response towards the target gas exposure, the conductance trend seems to be exactly comparable with those reported in the previous paragraphs. Also in this case a slow and incomplete recovery is observed.

The device recovery, even in absence of NO_2, suggests that the conductance variation is mainly related to the monotonous time-increasing of the number of

interacting molecules, continuously extracting a negative charge from the active film and resulting, in turn, in the observed time-dependant conductance improvement. Since in fact:

$$G = \frac{\mathrm{I}}{\mathrm{V}}$$

and

$$I(t) = \mathrm{Aqn(t)}$$

where q is the electron charge, A the interacting surface of the device, V the applied bias and $n(t)$ the reactive carrier density for surface and time unit that changes as function of the analyte concentration, the conductance is given by G(t)=Aqn(t)/V.

$$\mathrm{G}(t) = \frac{\mathrm{Aqn(t)}}{\mathrm{V}}$$

Now, being $n(t) = n_0 + \int_0^t C(t')dt'$, with n_0 the initial carrier density and $C(t)$ the analyte concentration, the signal could then be governed by the following equation[14]:

$$G(t) = G_0 + \alpha \int_0^t C_s(t')dt' \qquad (1)$$

where G_0 is the unperturbed conductance, $C_s(t)$ is the surface analyte concentration in the time window and α is a dimensional constant that takes into account the electron charge, the applied bias and the surface reaction rate constant. Here in eq. (1) it can be assumed, for the sake of simplicity, that during the interaction a single, unitary negative charge, is exchanged between film and analyte.

In addition, examining the entire measurement, a worsening of the conductance variation, calculated as usual $\Delta G/G_0$, is obtained, passing from 8% in the first exposure window to 3.3% in the third one. This phenomenon can find a possible explanation considering that GR sites likely remain partly occupied by the NO_2 molecules after each recovery step so that less sites could be available to subsequent sensing measurement. As a result, at fixed gas concentration, the response reduces progressively.

[14] This kind of equation is typically adopted to describe the so called integrating sensors that are characterized by the accumulation of the quantity determining the output.

With these points in mind, we were spurred to seek for a different operating way for our GR-based chemi-resistor. To do this, a new protocol (**Test3**) was defined (Fig. 4.6). Differently from the protocol**s** introduced so far, it consists of NO_2 pulses at different concentrations, followed by short recovery steps. For all concentrations, except for the exposure to 50 and 10 ppb, the protocol is set as follows:

- 2 minutes exposure to NO_2;
- 4 minutes flushing with carrier gas (N_2)

In the case of exposure towards inferior NO_2 concentrations, the only change regards the time window that requires 4 minutes to achieve an appreciable conductance variation since this parameter has been suggested to be proportional to the integral of concentration in the whole exposure time (eq. 1). Also, at the test start, the baseline lasts 15 min in order to better stabilize the device.

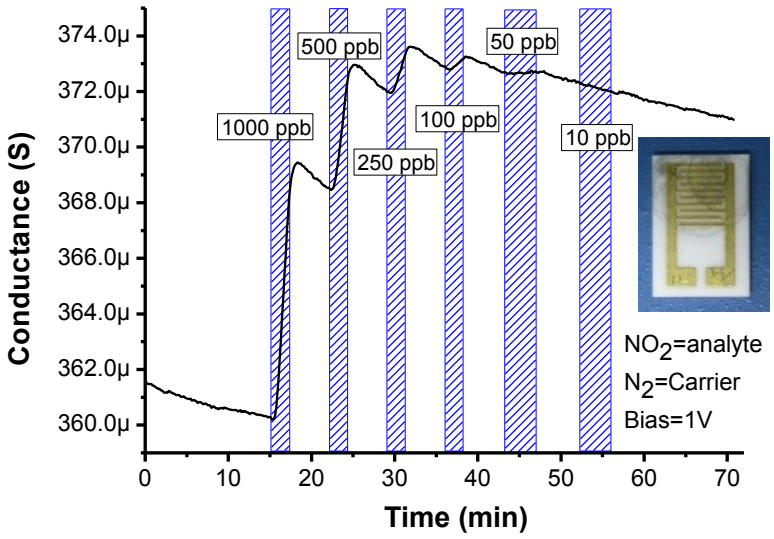

Fig. 4.6: conductance dynamic behavior of GR-based chemi-resistor as response upon protocol named Test3. It consists of sequential NO_2 pulses at different concentration levels (dashed blue areas) from 1000 ppb down to 10 ppb. Each pulse lasts 2 min apart from those at 50 ppb and 10 ppb that last 4 min in order to achieve an appreciable conductance variation. No conductance change is observed at 10 ppb. Inset: picture of tested GR-based chemi-resistor.

It is straightforward to observe that, for each NO_2 pulse, the conductance is characterized by the slope change as function of concentration level: it results to be steeper when the device is exposed to 1 ppm and becomes flatter during the exposure towards 50 ppb while the concentration of 10 ppb appears to be too much low to be detected. Accordingly, it is immediate to move the glance from the

conductance (or current) to the derivative of the signal itself because the slope observation could return information on the gas concentration and vice versa. Moreover, this simple and essential observation reveals so powerful that a series of device drawbacks can be circumvented. First of all, the derivative analysis allows to compare devices fabricated starting from different batches and/or having a large different parameters such as initial conductance and response to the analyte, as already discussed (Par 4.1.1). More importantly, the lack of the signal saturation (see Par. 4.1), the slow and incomplete recovery for GR-based gas sensors no more represent a limitation, since the derivative of the conductance signal provides all the information needed to correlate the device response to the analyte. As a result, the restoration of the signal to the initial conditions is no longer strictly required.

Looking at the eq. (1), this conjecture finds ulterior confirmation. The time derivative, in fact, is found to be directly proportional to the analyte concentration:

$$\frac{\partial G(t)}{\partial t} \propto C_s(\mathrm{t}) \tag{2}$$

suggesting that the first order time derivative of the device conductance is strictly connected only to the interacting analyte concentration and that this biunivocal correspondence could be advantageously exploited to correlate device response and analyte concentration itself (see next paragraph).

Therefore, the introduction of this innovative approach is of particular relevance to successfully overcome the herein presented limitations, such as recovery and devices reproducibility, which are related not only to GR-based devices but also to all solid state sensors. Last but definitively not least, the advantage of using such powerful analysis method lies in the possibility to calibrate the GR-based gas sensor in a narrow NO_2 concentration range.

4.3 Sensor calibration

An essential requirement for sensors is to provide correlation between input and output, being this procedure usually defined as calibration [89]. In this way, it is immediate to climb up to the input, knowing the output and vice versa.

In the case herein discussed, the derivative exploitation makes also possible the GR-based chemi-resistor calibration in the narrow NO_2 concentration range from 1 ppm down to 100 ppb.

In Fig. 4.7, the conductance dynamic behavior, previously shown in Fig. 4.6, is now reported overlapped to its derivative signal is. The derivative is calculated as the average of the incremental ratio according to the following relation implemented by OriginPro® software:

$$f'(x_i) = \frac{1}{2}\left[\frac{y_{i+1} - y_i}{x_{i+1} - x_i} + \frac{y_i - y_{i-1}}{x_i - x_{i-1}}\right]$$

where x_i and y_i are generic time instant and conductance value, respectively.

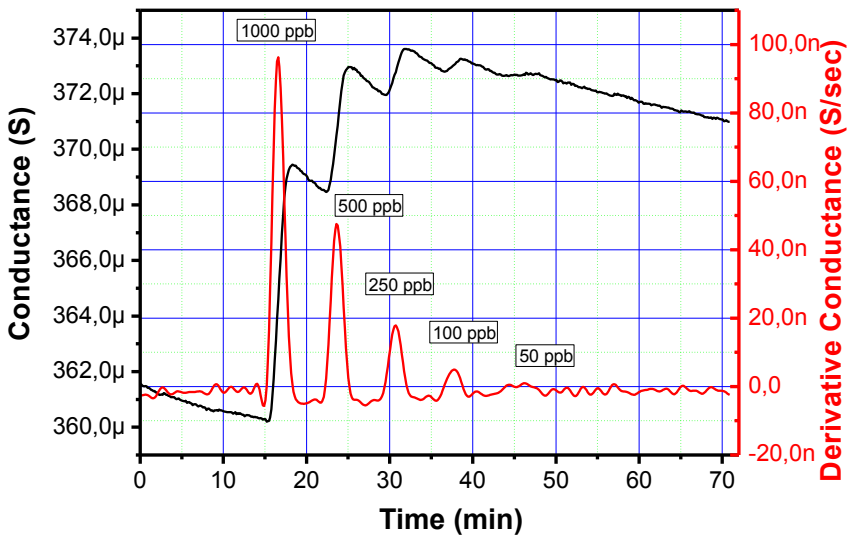

Fig. 4.7: conductance dynamic behavior of GR-based chemi-resistor as response upon protocol named Test3 (black line). Derivative of the conductance signal (red line).

The effects of the algorithm application on the signal are well-rendered: in sensor devices whose reaction kinetic is speed up by a fairly high working temperature, the t dependence in the equation (2) is rapidly lost and G(t) rapidly

attains a constant value, related to the analyte concentration in the testing environment. On the contrary, in devices operating at RT as in our case, during the target gas exposure, G(t) exhibits a maximum, which corresponds to the achievement of analyte maximum concentration on the sensing film surface. This is the reason for which the time derivative of the conductance signal presents as a sequence of maxima, strictly correlated to the analyte concentration: indeed the trend between the maxima and the concentration is fairly linear, also highlighting an increase of one order of magnitude passing from 100 ppb to 1000 ppb upon NO_2 exposure (Fig. 4.8).

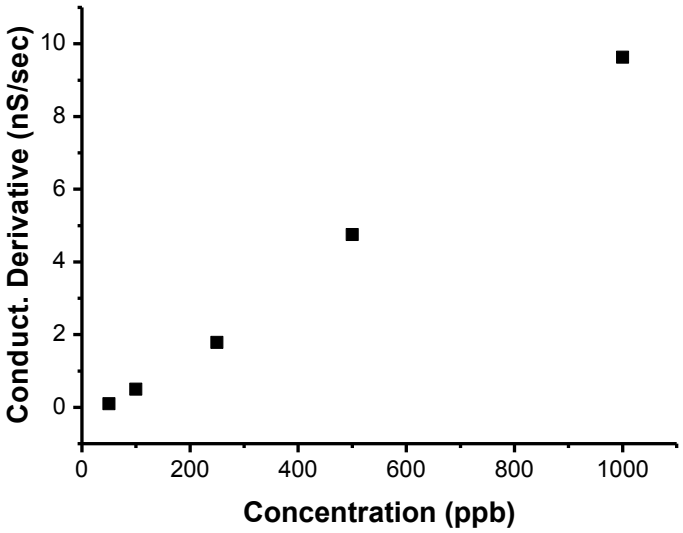

Fig. 4.8: maxima of conductance derivative reported in Fig. 4.7 as function of NO_2 concentration.

To further validate this result, the number of NO_2 pulses have been increased with respect to that shown in Fig. 4.8, using the same set up conditions, and the maxima were plotted vs the concentration in Fig. 4.9.

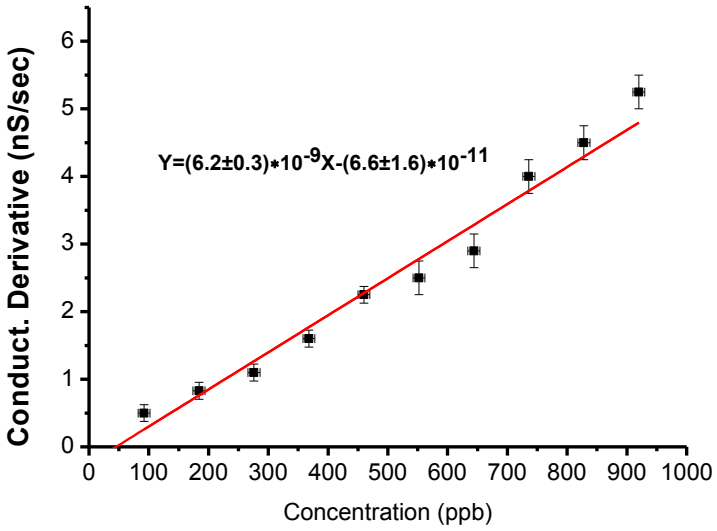

Fig. 4.9: calibration plot of graphene-based chemi-sensor towards NO_2 exposure. The red straight line fits the points of maximum of the signal derivative collected at different NO_2 concentrations. From the calibration curve, the sensor LOD and the sensitivity can be estimated: the LOD value is about 50 ppb, obtained intersecting the line with the abscissa; the sensitivity, defined as $\partial Y/\partial M$, where Y is the sensor output and M is the independent variable, corresponds to the curve slope, and is equal to $6.2 \cdot 10^{-9}$ S/(sec·ppb).

The result[15] highlighted by Fig. 4.9 permits to further prove two assessments: first of all, the validity of the theoretical model concerning the interaction between the analyte, as described by eq. (1); then, more importantly, eq. (2) is definitively confirmed and effectively the first order time derivative can be bi-univocally put in correspondence with the analyte concentration, providing a mean to successfully calibrate the GR-based gas sensor between 100 ppb and 1000 ppb. Notably, the result importance is borne out by the fact that, in eq. (1), the dependence from the gas concentration results not immediate, being involved in the integral for the whole exposure window.

Finally, through the calibration plot, two characteristic quantities of sensors can be estimated: the sensitivity and the limit of detection (LOD). The sensitivity is generally defined as $\partial Y/\partial M$, where Y is the sensor output and M is the independent variable[16]. LOD is the minimum amount of analyte that the sensor can be able to detect. As regards the examined sensor, in particular, the sensitivity corresponds to the straight line slope and is equal to $6.2 \cdot 10^{-9}$ S/(sec•ppb) while LOD is about 50

[15] The error bars in Fig. 4.9 have been calculated by considering the difference between two subsequent points in the neighborhood of the maximum for each derivative peak. Regarding the concentration levels, the uncertainty is determined by the NO_2 bottle supplier.

[16] Since the sensitivity can be calculated for each kind of sensor, Y and M can be whatever output and input variables, respectively.

ppb. Despite of this value derives from an extrapolation, Figs. 4.6-4.7 show that the signal and its derivative are fairly distinguishable from noise at 50 ppb, differently from what happens at lower concentration level.

To the best of our knowledge, in the literature there are no GR-based sensors operating in environmental conditions able to achieve the detection of NO_2 in the sub-ppm range [4, 10, 24], except for the work of Chen et al.; in that paper, they report on the record gas detection of parts per trillion (ppt), nevertheless such a remarkable result is accomplished by operating in particular conditions, namely in inert atmosphere and continuously refreshing the sensor surface by pumping UV light in situ [25].

4.4 Preliminary results towards other analytes

Once we have reached the essential goal to detect the concentration down to 50 ppb of NO_2 with the sensor operating in environmental conditions, we would like to go deeply and try to answer to the question: could this sensor be sensible to other analytes? To this aim, the sensor has been put again through **Test1** towards other two different analytes, NH_3 and H_2 [17](Fig. 4.10), always setting RH=50% and RT.

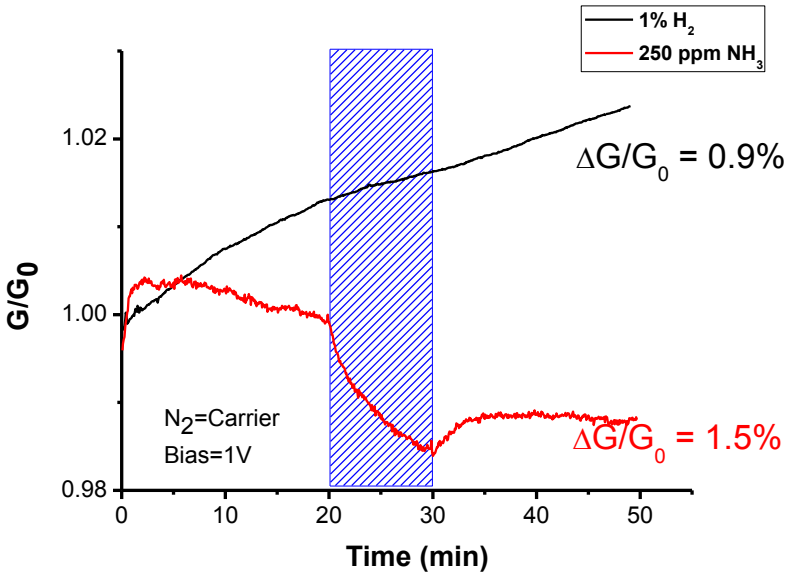

Fig. 4.10: normalized electrical conductance behavior of chemi-sensors towards NH_3 (red line) and H_2 (black line). The sensor seems to be almost insensitive to H_2 and has an extremely small signal variation upon NH_3 especially if compared with NO_2 exposure (see Fig. 4.4). The H_2 concentration has been chosen in order to test the sensor at a level quite far from the limit of inflammability in air, that is around 4%.

Fig. 4.10 shows that the sensor does not produce a remarkable signal variation during the H_2 exposure (black line) and, when the gas flow is stopped, the sensor does not recover at all. Also the interaction with ammonia generates an extremely small signal variation, especially if compared with that reported in Fig. 4.4 towards NO_2. Indeed, once more again, on one side, the strong specificity of this GR-based gas sensor at NO_2 is confirmed, on the other hand the answer to the starting question seems to have a negative answer.

[17] For realistic applications of the device under test, the level of H_2 concentration has been set at 1%, since the H_2 limit of inflammability in air is approximately 4% [Assembly of thermally reduced graphene oxide nanostructures by alternating current dielectrophoresis as hydrogen-gas sensors].

In the literature, instead, several works have theoretically proved that different types of GR functionalizations could help to solve this problem [1, 10, 99] and GR-metal nanoparticles (GR/MNPs) hybrids seem to be very interesting candidates [99-101].

In Fig. 4.11, the first preliminary results of GR-based sensors functionalized with Pd and Ag nanoparticles are reported. In Panel (a), the comparison between conductance variation of GR-PdNPs based chemi-resistor towards the three analytes is shown, while in Panel (b) the same comparison is carried out for device based on GR functionalized with Ag NPs.

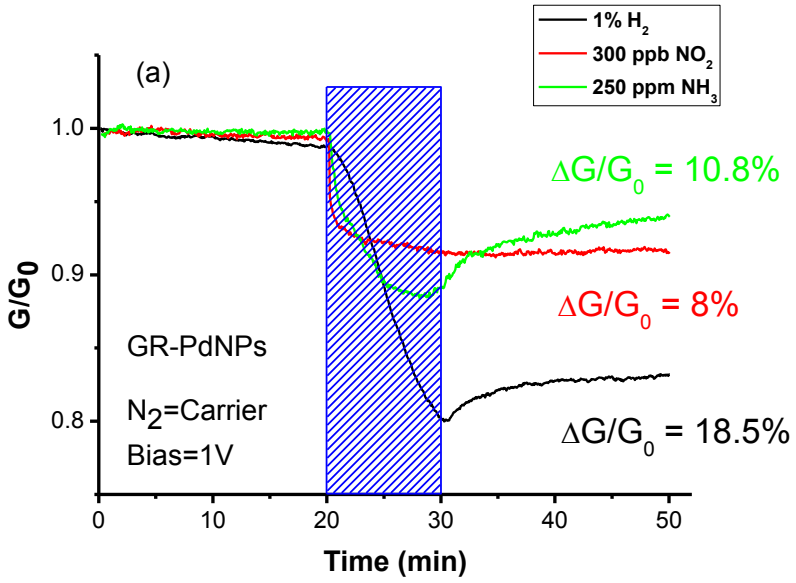

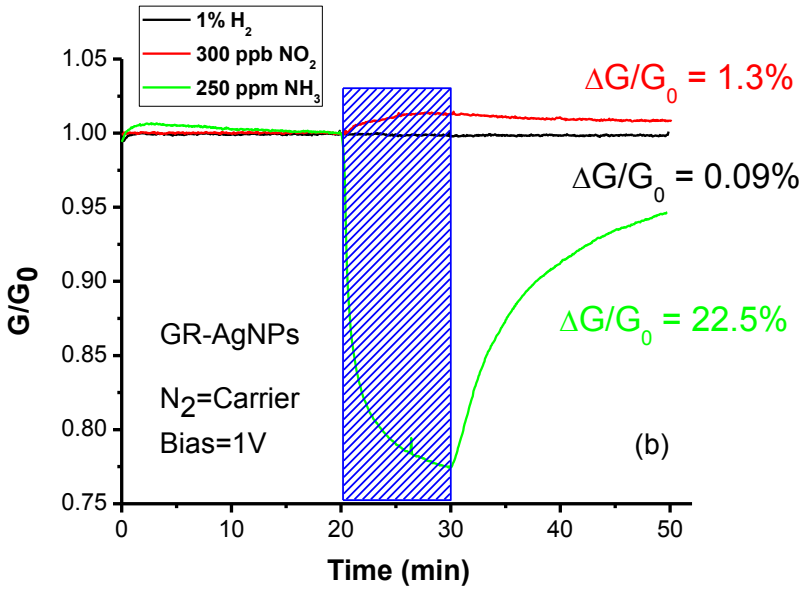

Fig. 4.11: normalized electrical conductance behavior of the chemi-sensor based on GR functionalized with (a) Pd and (b) Ag nanoparticles towards H_2 (black line), NO_2 (red line) and NH_3 (green line). GR-PdNPs and GR-AgNPs are strongly specific to H_2 and NH_3, respectively, while the conductance variation towards the other two analytes are much less pronounced.

With respect to the pristine GR (Fig. 4.10), GR-PdNPs and GR-AgNPs, exhibit a greater specificity towards H_2 and NH_3, respectively. The results reveal particularly promising and encouraging because, apart from the specificity modulation towards other analytes, the functionalization procedure has been successfully employed for the first time on LPE GR; in the literature, instead, most of the research groups have recourse to rGO and GR grown by CVD or by SiC thermal decomposition [100, 102-103]. Therefore, these results could pave the way to investigate the functionalization with other MNPs in order to detect other dangerous molecules [1].

4.5 Chemi-resistor based on CVD grown graphene

The achievement of the aforementioned outstanding findings has spurred me to better understand their origin in order to further improve the performances. Thus, exploiting the assessments concerning the material characterization (see Chapter 3), the comparison between LPE GR-based sensor and a chemi-resistor based on CVD GR has been employed. This part of experimental activity has been conducted at the Electronic Components, Technology and Materials Laboratory of the Delft Institute of Microsystems and Nanoelectronics.

The device has been realized by transferring CVD grown GR on IDE prepared by lithography (Fig. 4.12). The gold fingers are spaced of about 3 μm so that the GR flakes, that are almost 10 μm in size, surely close the contacts. The transfer procedure from the Cu substrate to the bare structure has been detailed in Paragraph 3.3.

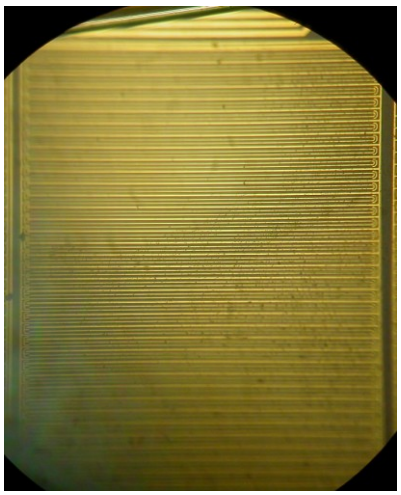

Fig. 4.12: gold interdigited electrodes showing the bare structure for the resistor based on CVD grown GR.

After the GR film deposition, a volt-amperometric characterization is performed (Fig. 4.13) in order to verify the effectiveness of the contacts realization as well as their ohmicity.

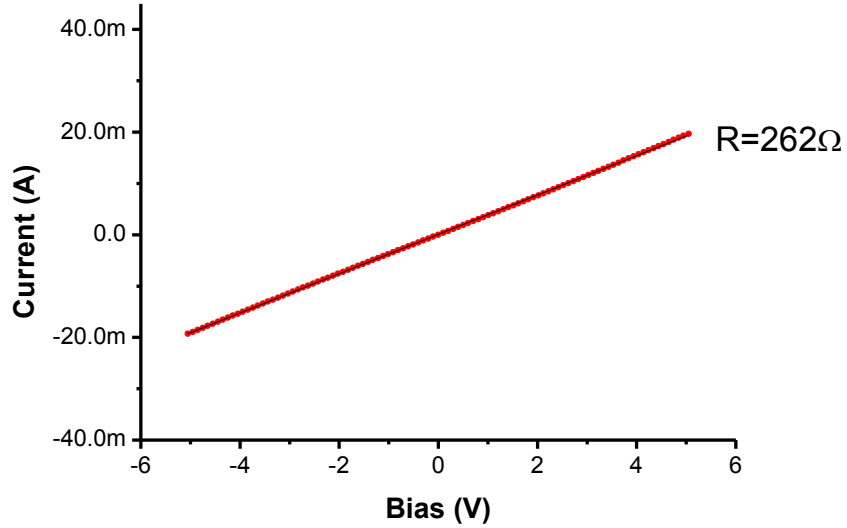

Fig. 4.13: I-V plot for resistor based on CVD grown GR. From the curve fit a resistance value equal to 262 Ω is determined.

By fitting the data, a resistance equal to 262 Ω can be extrapolated, indicating a quite good adhesion between GR flakes and fingers, whereas the symmetric behavior of the volt-amperometric characteristic testifies the ohmic nature of the GR/Au junction. Also, the strong conductivity of the material further proves the presence of SLG on the fingers (see Table 2.1).

Such prepared device has undergone **Test1** such as in Fig. 4.3, with the equipment operating in the same environmental conditions previously described.

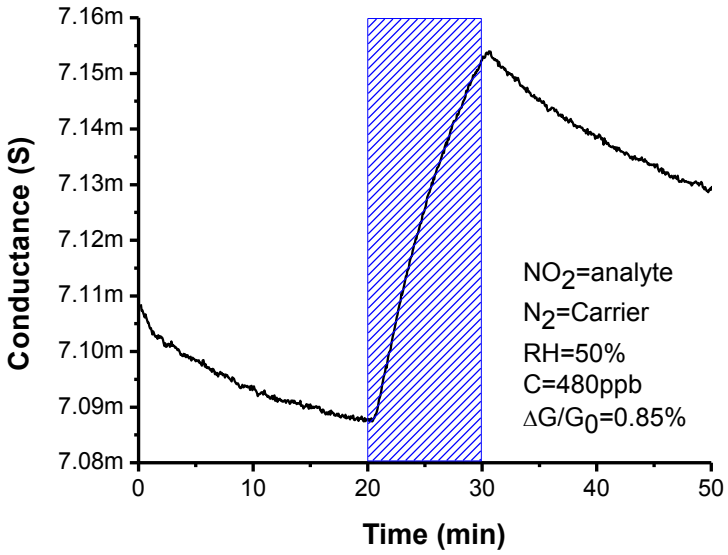

Fig. 4.14: dynamic response of a chemi-resistor based on CVD grown GR towards 480 ppb of NO_2. A conductance variation, $\Delta G/G_0$, is calculated as equal to 0.85%.

Analyzing the graph depicted in Fig. 4.14, analogies and differences with respect to the other sensor can be noticed. An appreciable current variation (0.85%) has been recorded upon NO_2 exposure to 480 ppb. The LPE GR-based sensor, instead, was able to achieve values up to 33% towards 350 ppb. In addition, the high conductivity and, in turn, the current in the range of few mA depends on the different morphology of the CVD GR with respect to LPE one. The perfect planar structure of the graphene grown by CVD, in fact, and the absence of ripples on the flakes surface make easier the current flow than in the more complex morphology of the LPE deposited material. These differences are also borne out by the slower kinetics during the exposure window if compared to that reported in Fig. 4.4, for instance.

The investigations on the material presented in the previous Chapter lead to address these phenomena to the GR flakes composition and to the film arrangement. Here, the goal is to find further proofs for this thesis.

The analogy with the LPE graphene based device lies instead in the direction of the response variation to NO_2, since also in this case an increase of the conductance is observed, indication of the occurrence of a p-type doping also for the material produced by means of CVD. Furthermore, despite of the slightly tilted baseline, also this device shows a partial and slow recovery.

As far as the device is concerned, the first purpose is to evaluate the performances reproducibility. To this aim, **Test2** has been accomplished on the device, by repetitively exposing the device towards the same analyte concentration, in this case 480ppb of NO_2.

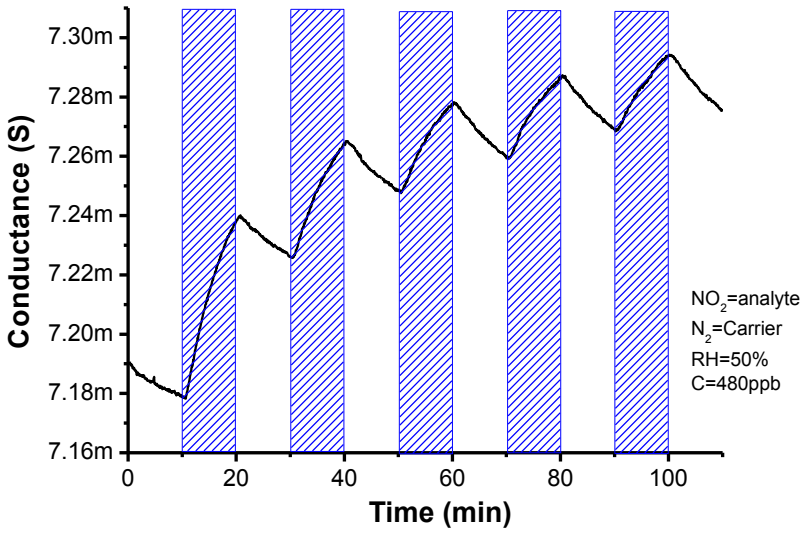

Fig. 4.15: current dynamic behavior of CVD GR-based chemi-resistor as response upon protocol consisting of five sequential exposure towards 480 ppb of NO_2 (dashed blue areas). Except the first step ($\Delta G/G_0$=0.8%), equal variations of the current are observed in the following steps ($\Delta G/G_0$=0.4%). The disagreement is likely due to the adaption of the device to the test chamber conditions.

In Fig. 4.15, except the first step, in which a conductance variation equal to 0.8% is calculated, the other data are comparable, being 0.5% in the second step and 0.4% in the last three ones. The reason for the difference between the first and the other steps can be likely explained by considering the delay for the device adaption to the test chamber conditions. Therefore, the device performances towards NO_2 detection can be assumed quite reproducible.

Once this crucial point has been certified, the test for the device calibration has been performed. This protocol (**Test4)**, similar to **Test3**, consists of NO_2 exposures at different concentrations, followed by recovery steps. In particular, the protocol is set as follows:

- 2 minutes exposure to NO_2;
- 20 minutes flushing with carrier gas (N_2)

Due to the slight current variation recorded in the previous tests, a wider range of concentrations, from 2400 ppb down to 240 ppb, has been taken into account compared with that in **Test3** (Fig. 4.6). The measurement has been repeated two times (black and red lines in Fig. 4.16) in order to prove the performance reproducibility also for this test.

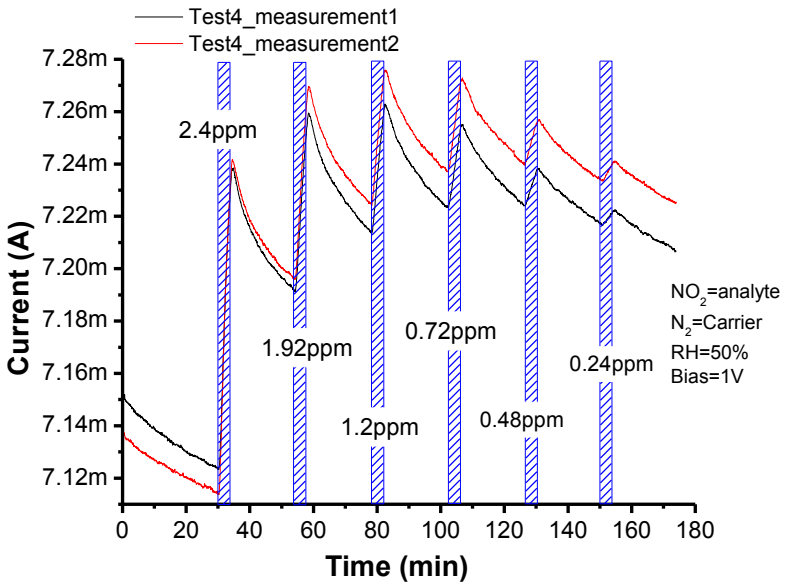

Fig. 4.16: current dynamic behavior of CVD GR-based chemi-resistor as response upon protocol named Test4. It consists of sequential NO_2 pulses at different concentration levels (dashed blue areas) ranging from 2400 ppb down to 240 ppb. Each exposure step was 2 min long, preceded and followed by 20 min long baseline and recovery phases, respectively, in inert atmosphere.

The dynamic behaviors in Fig. 4.16 clearly exhibit repeatable measurements, as showed by the inset in Fig. 4.17 where the current variations for cycles in Fig. 4.16 are reported. The experimental data are fairly overlapped.

By plotting the conductance variation as function of the concentration, a linear relationship is observed (Fig. 4.17). To a first analysis this behavior could appear inconsistent with the model discussed in section 4.2 to explain the linearity between the time derivative of conductance and analyte concentration. Nevertheless, noting that in the case of CVD GR-based sensor the exposure to about the same concentration of analyte produces a variation of conductivity of over one order of magnitude lower than that of LPE GR-based chemi-resistor, this suggests that the conductance signal variation can be approximated to the first derivative, thus justifying the linearity with the analyte concentration. In this case, the sensor calibration can be properly carried out by correlating the variation of conductance to the NO_2 concentration.

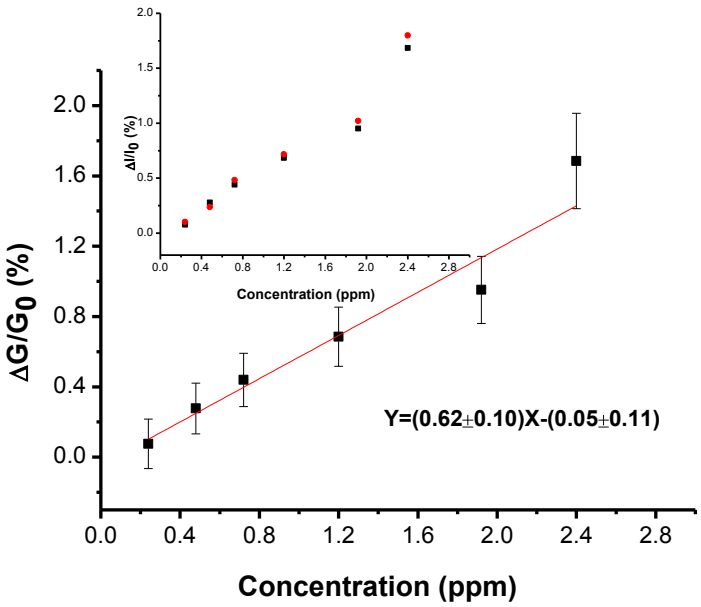

Fig. 4.17: calibration plot of CVD graphene-based chemi-sensor towards NO_2 exposure. The sensitivity is estimated as 0.6%/ppm whereas the LOD is roughly 600 ppb. Inset: current variations for cycles in Fig. 4.16 showing agreement between the two data set.

Fig. 4.17, allowing the calculation of sensitivity and LOD, definitively fills the frame of the comparison between the two types of chemi-resistors and, in general, between the LPE and CVD GR. The sensitivity is determined to be 0.6%/ppm whereas the LOD[18] is approximately 600 ppb that is roughly 10 times higher than the value extrapolated for LPE GR-based chemi-sensor.

This result, jointed to findings regarding Fig. 4.14 and to materials characterizations, notably proves that the flake structure plays a key role in the sensing properties. As such, the LPE GR-based sensor differs from the CVD GR-based one for the material composition. In the latter case, in fact, because of the flake size in the micrometric range, the density of edges at fixed area of GR film is remarkable reduced. In turn, the surface of the flakes is predominant and is mostly involved in the interactions with the analyte molecules. However, both the lower values of current variation at comparable NO_2 concentrations and the LOD here reported attest that the boundaries result to be much more reactive with respect to the flake plane. The contribution of the edges in the sensing properties could be also testified by the linear relationship of $\Delta G/G_0$ versus the NO_2 concentration since the basal planar structure has surely a different behavior with molecule analytes in comparison with the edges.

[18] The LOD is calculated as $LOD = 3S_D/m$, where m is the slope of the calibration curve and S_D is the standard deviation of noise in the presence of the only carrier gas.

4.6 Conclusions

In this Chapter, all aspects concerning the chemi-sensors prepared with LPE GR interacting with NO_2 and operating in environmental conditions (i.e. RT, pressure and in presence RH) have been investigated.

The sensor has been firstly demonstrated to be stable in these conditions, then to be able to achieve a signal variation up to 33% in the single sensing measurement towards 350 ppb of NO_2, this concentration being in agreement with the limits imposed by the European rules for NO_2 (see Chapter 1).

Also the issue related to the devices reproducibility is addressed. Because the drop casting deposition technique can be affected by lack of homogeneity of GR suspension onto the alumina substrate, some differences from device-to-device performance could be obtained, even if the feed solution comes from same batches.

The gas sensors, similarly to all solid state sensors, suffer the absence or slow return to the initial conditions after the signal output. Various routes have been run in order to circumvent this drawback. Firstly, an easy and original method to refresh the exhaust GR-based chemi-sensors has been introduced, simply exploiting the strong solubility of NO_2 in water. The approach, consisting in dipping the device into hot water, reveals so effective that devices fully insensitive to NO_2 due to intentional poisoning effects return to the initial conditions, leading to performances even better than those obtained when the devices were soon prepared.

Then, a more powerful solution has been presented. Instead of analyzing the sensor output as response to the gas exposure, the signal derivative has been taken into account. This has allowed to successfully overcome the limitations already discussed. Regarding the devices reproducibility, the derivative analysis allows to compare devices based on materials coming from different batches and/or having a huge range of different parameters. As concerns the absence and the slow recovery, the method permits to avoid the return at the initial conditions since only the output derivative can be exploited. Finally, the methodology seems particularly attractive since it provides a mean to strictly correlate the conductance derivative to the analyte concentration in the extremely narrow concentration range from 1000 ppb down to 100 ppb, making this device one of the first calibrated GR-based chemi-sensor for NO_2 presented in the literature able to work in environmental conditions.

The sensor has been made sensitive to other analytes, H_2 and NH_3, functionalizing for the first time in the literature LPE GR with Pd and Ag nanoparticles. The results appear particularly promising since pristine GR was almost fully insensitive to the same analytes.

Finally, the chemi-resistor based on CVD grown GR has been introduced. The volt-amperometric characterization has showed the success in the device preparation by transferring on IDE CVD grown GR. Through the comparison of the sensors performance in NO_2 detection, the role of the material defects, particularly edges defects, have been addressed. In fact, for the sensor based on LPE GR, having a much higher density of defects edge, LOD equal to 50 ppb has been determined. CVD GR-based sensor, instead, has exhibited LOD of approximately 600 ppb since the GR film basically consists of larger flakes and especially the surface is involved in the adsorption phenomenon rather than boundaries.

APPENDICES

A. Alumina transducer details

In this section, the information regarding the alumina transducer used as substrate for the chemi-sensors (see Chapter 4) are reported.

The sketch is depicted in Figure A1.

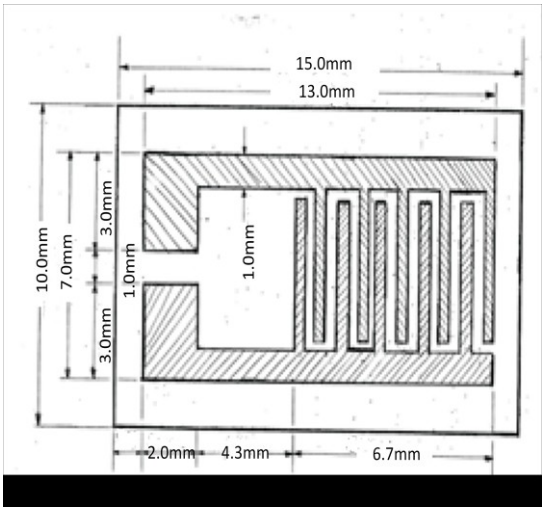

Fig. A1: Sketch of transducer used as substrate for chemi-sensor

All the finger dimensions have been designed by ourselves and customized by 3M taking into account our need and the structure of the Gas Sensor Characterization System (see Appendix B). The GR film covers the Au interdigited electrodes (IDE) for an area of about 49 mm^2.

Because the devices have been used as chemi-resistors, volt-amperometric measurements have been performed by applying the two probes on the larger pads of the transducer. The probes have a diameter of about 500 μm [3].

B. Gas Sensor Characterization System

The Gas Sensor Characterization System (GSCS) employed in the ENEA-MDB lab has been designed by ENEA researchers and customized by Kenosistec.

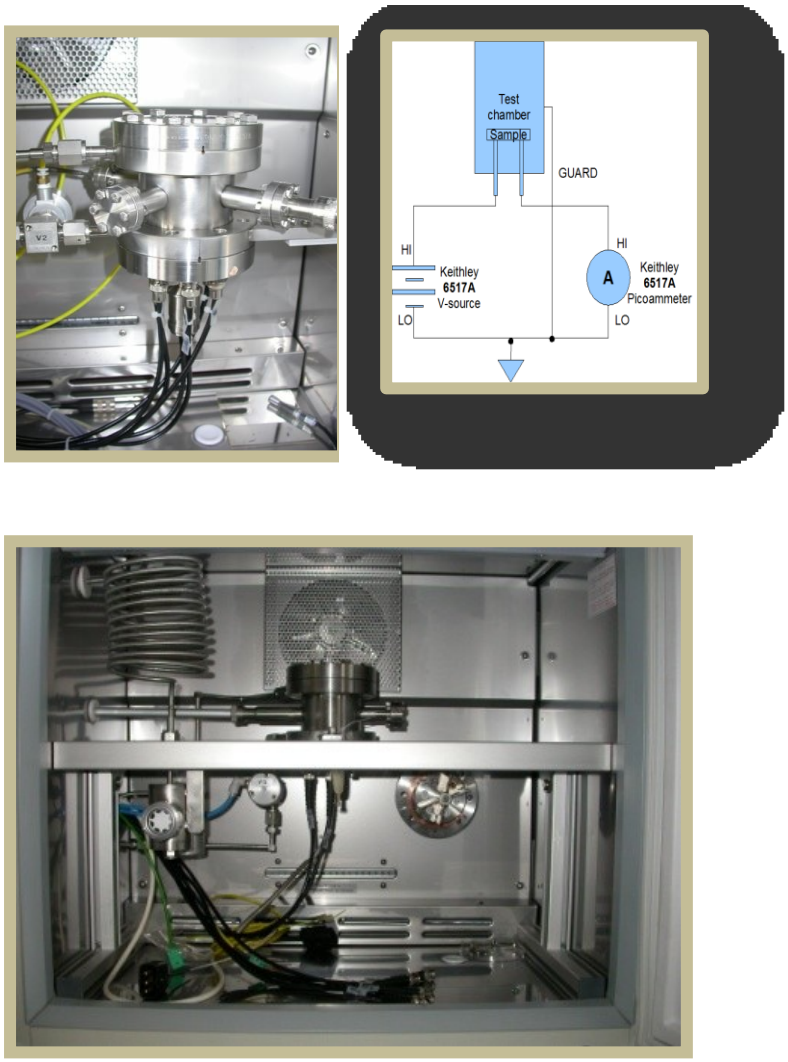

Fig. B1: Pictures of Gas Sensor Characterization System and corresponding circuital scheme.

The sensor device is located in a stainless steel test chamber (see Fig. B1) placed in a thermostatic box. The chamber is provided of an electrical grounded connector for bias and conductance measure as shown on the right in Fig. B1.

A constant flow (500sccm) of the gas carrier, i.e. N_2 crosses the test chamber. The carrier can be properly humidified through a water bubbler placed in a thermostatic bath. In this environment, characterized by controlled temperature and humidity, the conductance value of the device in its equilibrium state is firstly measured and this step represents the so called baseline; after that, an intentional

disruption of the equilibrium state is produced by introducing the analyte gas in a controlled amount and by mixing it with the carrier gas via pneumatic valves and through programmable Mass Flow Controllers. Because the concentrations needed to be detected are in the range of hundred ppb, this poses a fundamental issue in reproducing as much as possible these conditions in lab. In addition, the reproducibility of these levels of concentration in the lab equipment appears no immediate since the pipes and the core of test chamber is made of electro-polished stainless steel. This means that the NO_2 molecules can spread over and adhere also to the chamber walls, reducing the effective analyte concentration interacting with the sensor. In order to minimize the effects of these limitations, within 30 minutes before the measurements, the maximum available concentration of NO_2 is fluxed into the chamber for 15 minutes through a protocol controlled via software. In order to check the degree of agreement between the gas concentrations set in the protocols and those present into the chamber, tests have been performed through an FTIR (THERMO ANTARIS IGSS) equipped with a cryogenic detector and a cell having an optical path equal to 10 m. All these operations guarantee the reproducibility of the condition of the test chamber. Hardware and software implemented on a work station allow to control and record environmental parameters, device bias and output signal, making possible to perform customizable automated tests on devices (Protocols).

C. Abbreviations and acronyms

Here below a list of the mostly used abbreviations and acronyms in the text is reported.

AB	Anodic Bonding
AFM	Atomic Force Microscopy
AQG	Air Quality Guidelines
CNTs	Carbon nanotubes
CNP	Charge Neutrality Point
CVD	Chemical Vapor Deposition
DLS	Dynamic Light Scattering
DMF	Dimethylformamide
EPA	Environmental Protection Ambient
EU	European Union
FLG	Few-Layer Graphene
h-BN	hexagonal Boron Nitride
FWHM	Full Width at Half Maximum
GO	Graphite Oxide
GP	Gel-pak elastic sheet
GR	Graphene
GR/AgNPs	Graphene-silver nanoparticles
GR/PdNPs	Graphene-palladium nanoparticles
GR/MNPs	Graphene-metal nanoparticles
HF	Hydrofluoric acid
HNO_3	Nitric acid
HOPG	Highly-Oriented Pyrolitic Graphite
IDE	Interdigitated Electrodes
IPA	Isopropylic alcohol
LOD	Limit Of Detection
LPE	Liquid-Phase Exfoliation
ME	Micromechanical Exfoliation
MOX	Metal Oxide
NA	Numerical Aperture

Nd:YAG	Neodymium-doped yttrium aluminum garnet
NEMS	Nano-ElectroMechanical System
NIOSH	National Institute for Occupational Safety and Health
nLG	Number of graphene layers
NMP	N-methyl-pyrrolidone
OSHA	Occupational Safety and Health Administration
PC	Polycarbonate
PDMS	Polydimethylsiloxane
PEL	Permissible Exposure Limit
PM	Particulate Matter
PMMA	Polymethylmethacrylate
PPB	Parts Per Billion
PPM	Parts Per Million
PPT	Parts Per Trillion
rGO	Reduced Graphene Oxide
RT	Room Temperature
sccm	Standard cubic centimeter
SEM	Scanning Electron Microscopy
SiC	Silicon carbide
SiO_2	Silicon Dioxide
SLG	Single-Layer Graphene
SNR	Signal to Noise Ratio
STEL	Short-Term Exposure Limit
TEM	Transmission Electron Microscopy
THF	Tetrahydrofuran
3D	Three-dimensional
TMDC	Transition Metal Dichalcogenide
2D	Two-dimensional
TWA	Time-Weighted Average
UHV	Ultra-High Vacuum
VOCs	Volatile Organic Compounds
WHO	World Health Organization

CONCLUSIONS

The present thesis work was focused on two major items: 1. preparation and characterization of GR films; 2. test of the material sensing properties towards analytes by employing GR-based chemi-resistors as transducers.

As regards the material synthesis, a brief survey on the growth techniques present in the literature and the related peculiarities were reported . In this work, the mostly exploited techniques for the GR production were LPE and CVD.

The liquid phase exfoliation of graphite down to FLG and SLG was achieved preparing two types of suspension. The first one was realized by using a green solvent, i.e. a mixture of H_2O and IPA, in volumetric ratios 1:5. This recipe, presented for the first time in the literature, was mainly developed with the purpose to find an eco-friendly and no-toxic solvent for the production of GR layers: the goal was successfully achieved by performing a study both on the solvents thermodynamic property and the physicochemical parameters.

The second GR suspension was prepared exfoliating graphite in NMP, in order to demonstrate that the hydro-alcoholic mixture provides comparable results to those obtained by means of this most common solvent . By means of DLS and Raman characterizations, the perfect equivalence between the two GR suspensions was demonstrated, in terms of yield and mean flakes lateral size, that is in the range of few hundred nanometers, similarly to values reported in the literature. The flake dimensions were confirmed through TEM and AFM characterizations. The Raman analysis also allowed to infer that LPE material is composed by flakes with number of layers equal or less than five. In addition, Raman spectra information on the presence of some defects that TEM and AFM disclosed to be due to the edges of flakes.

As far as CVD technique is concerned, the recipe for GR growth was presented as well as all steps of the optimized transfer procedure. To this respect, three requirements were basically taken into account: the preservation of the GR film integrity and cleanness; the achievement of flakes size as large as possible; the possibility to perform the overall process in the shortest time possible. For instance, the etching time of the growth substrate (Cu) as function of the $FeCl_3$ dilution was reduced from 17-18 hours down to 9-10 hours, obtaining also the calibration curve

for this parameter. Raman Spectroscopy on CVD GR proved both the successful achievement of SLG growth on Cu and the transfer of large, clean flakes on SiO_2/Si. The typical lateral sizes were in the range of few ten micrometers, as certified by AFM measurements. The comparison of CVD GR spectrum with ME one, that I discussed in my master thesis, showed the extremely high quality of the former. By cross-checking the characterization results for material synthesized by the two different methods, the nature of defects for LPE GR was definitively uncovered as due to the flake boundaries. In turn, this further confirms the lack of crystalline imperfections.

The sensing properties of the GR layers synthesized according the two different ways were investigated by testing GR based chemi-resistors towards NO_2. This specie was taken into account since it is associated with adverse effects on the human health and the air pollution. To this aim, the sensors were tested in environmental conditions, i.e. RT, pressure and in presence of RH, towards low concentration levels. In fact, a survey on the international concentration ranges to not exceed and on the exposure limits demonstrated that the general aim is to find routes and tools to make possible the detection and measurement of gases at levels of ppm and also lower. For instance, the LPE GR-based device was able to achieve a signal variation up to 33% during a single measurement towards 350 ppb of NO_2, this concentration being in agreement with the limits imposed by the European rules.

Because this gas sensor, similarly to all solid state sensors, suffers the absence or slow return to the initial conditions after the signal output, various routes were run in order to circumvent this drawback. Firstly, an easy and original method to refresh the exhaust GR-based chemi-sensors was introduced, simply exploiting the strong solubility of NO_2 in water. The approach, consisting in dipping the device into hot water, revealed so effective that devices fully insensitive to NO_2 returned to the initial conditions. Then, a more powerful solution was presented consisting in the analysis of the signal derivative instead of the sensor output as response to the gas exposure. This allowed to successfully compare devices based on materials coming from different batches and/or having a huge range of different parameters. As concerns the absence and the slow recovery, the method permitted to avoid the return at the initial conditions since all the information are involved in the derivative. The methodology provided a mean to strictly correlate the

conductance derivative to the analyte concentration in the extremely narrow concentration range from 1000 ppb down to 100 ppb. To the best of our knowledge, in the literature there are no GR-based sensors operating in environmental conditions able to achieve the detection of NO_2 in the sub-ppm range.

The sensor was made sensitive to other analytes, such as H_2 and NH_3, functionalizing for the first time in the literature LPE GR with Pd and Ag nanoparticles. The preliminary results appeared particularly promising since pristine GR was almost fully insensitive to the same analytes. These outstanding performances were easily explained by considering the large density of edge defects that are more reactive towards analyte interaction than the flakes surface. This assessment was further proved by comparing the performances of LPE GR-based chemi-sensor with the device based on CVD grown GR. Such prepared material, having flakes few orders of magnitude larger in size with respect to LPE GR, offers more surface prone to the interaction with the analyte molecules and, in turn, the density of edges at fixed area of GR film is remarkable reduced. Several experimental data attested this result. Firstly, the second sensor showed an appreciable current variation equal to 0.85% upon NO_2 exposure to 480 ppb while the first sensor reached values up to 33%. Then, CVD GR-based sensor exhibited LOD of approximately 600 ppb that is roughly 10 times higher than the value extrapolated for LPE GR-based chemi-sensor. Finally, the contribution of the edges could be also testified by the linear relationship of $\Delta G/G_0$ versus the NO_2 concentration, in the range from 2400 ppb down to 240 ppb, since the planar morphology has surely a different behavior with molecule analytes in comparison with the edges.

In summary, in this work the GR flakes morphology was addressed and demonstrated to play a key role in the gas sensing. Through GR-based sensors, the NO_2 detection in the sub-ppm range was achieved operating in environmental conditions.

SCIENTIFIC PRODUCTION

1. *B. Alfano, T. Polichetti, M. Mauriello, M. L. Miglietta, F. Ricciardella, E. Massera and G. Di Francia:* Modulating the sensing properties of graphene through an eco-friendly metal-decoration process (submitted to Sensors and Actuators B).

2. *F. Ricciardella, B. Alfano, F. Loffredo, F. Villani, T. Polichetti, M. L. Miglietta, E. Massera and G. Di Francia:* Inkjet printed graphene-based chemi-resistors for gas detection in environmental conditions. IEEE Xplore, *AISEM 2015, Feb 3-5, Trento (IT)* (submitted).

3. *M. A. Nigro, G. Faggio, T. Polichetti, F. Ricciardella, F. Fedi, M. L. Miglietta, E. Massera and G. Di Francia: Cross interference effects between water and NH_3 on a sensor based on graphene/silicon Schottky diode.* IEEE Xplore, *AISEM 2015, Feb 3-5, Trento (IT)* (submitted).

4. *B. Alfano, T. Polichetti, M. Mauriello, E. Massera, M. L. Miglietta, F. Ricciardella and G. Di Francia:* Tailoring the selectivity of chemical sensors based on graphene decorated with metal nanoparticles. IEEE Xplore, *AISEM 2015, Feb 3-5, Trento (IT)* (submitted).

5. *S. Rao, M. Gioffrè, T. Napolitano, E. Massera, M.A. Nigro, B. Alfano, T. Polichetti, F. Ricciardella, M. Mauriello, L. De Stefano, F.G. Della Corte, G. Di Francia, P. Delli Veneri:* Improving the gas sensing performance of chemiresistors by LED irradiation. IEEE Xplore, *AISEM 2015, Feb 3-5, Trento (IT)* (submitted).

6. *F. Fedi, M. L. Miglietta, T. Polichetti, F. Ricciardella, E. Massera and G. Di Francia:* A study on the physicochemical properties of hydroalcoholic solutions to improve the direct exfoliation of natural graphite down to few-layers graphene. *Material Research Express* ***2,*** *035601 (2015).*

7. *F. Ricciardella, E. Massera, T. Polichetti, M. L. Miglietta and G. Di Francia:* A calibrated graphene-based chemi-sensor for sub parts-per-million NO_2 detection operating at room temperature. *Applied Physics Letters* ***104,*** *183502 (2014).*

8. *T. Polichetti, F. Ricciardella, F. Fedi, M. L. Miglietta, R. Miscioscia, E. Massera and G. Di Francia, M. A. Nigro, G. Faggio, A. Malara and G. Messina:* Graphene-Si Schottky diode in environmental conditions at low NH_3 ppm level, *IEEE Xplore, pp. 23-26, DOI: 10.1109/NMDC.2014.6997412 (2014).*

9. *T. Polichetti, F. Ricciardella, F. Fedi, M. L. Miglietta, R. Miscioscia, E. Massera, S. De Vito and G. Di Francia, M. A. Nigro, G. Faggio, A. Malara and G. Messina:* Graphene-based Schottky device detecting NH_3 at ppm level in environmental conditions, *Procedia Engineering* ***87,*** *232 (2014).*

10. *F. Fedi, F. Ricciardella, M. L. Miglietta, T. Polichetti, E. Massera and G. Di Francia:* A simple method to recover the graphene-based chemi-resistors signal, *Journal of Sensors and Sensor Systems* ***3,*** *241 (2014).*

11. *F. Fedi, F. Ricciardella, M. L. Miglietta, T. Polichetti, E. Massera and G. Di Francia:* Easy recovery method for graphene-based chemi-resistors, *A. D'Amico et al. (eds.), Sensors and Microsystems: AISEM 2014 Proceedings, Lecture Notes in Electrical Engineering* ***109,*** *121, Springer Science + Business Media, LLC 2014.*

12. *F. Fedi, F. Ricciardella, T. Polichetti, M. L. Miglietta, E. Massera and G. Di Francia:* Exfoliation of graphite and dispersion of graphene in solutions of low boiling point solvents for use in gas sensor, *Proceedings of Sensors and Microsystems: AISEM 2013, Feb 5-7, Brescia (IT), pp. 143-147 (2013).*

13. *E. Massera, M. L. Miglietta, T. Polichetti, F. Ricciardella and G. Di Francia:* Reproducibility of the performances of graphene based gas sensitive chemiresistors, *Proceedings of Sensors and Microsystems: AISEM 2013, Feb 5-7, Brescia (IT),pp. 121-125 (2013).*

14. *F. Fedi, F. Ricciardella, M. L. Miglietta, T. Polichetti, C. Del Barone:* Analisi mediante Microscopia a Trasmissione Elettronica (TEM) di nanocristalli di grafene. *Rapporto tecnico n^o 0001724 del 25 Luglio 2013 (CNR/ICTP-ENEA).*

15. *L. Lancellotti, E. Bobeico, A. Capasso, M. Della Noce, P. Delli Veneri, S. Del Sorbo, T. Dikonimos, G. Di Francia, N. Lisi, A. Mittiga, T. Polichetti, F. Ricciardella:* Graphene/Silicon Heterojunction for Photovoltaic Applications, *Proceedings of 28th EUPVSEC, Paris 30 Sept – 4 Oct 2013, 340.*

16. *L. Lancellotti, T. Polichetti, F. Ricciardella, O. Tari, S. Gnanapragasam, S. Daliento and G. Di Francia:* Graphene applications in Schottky barrier solar cells, *Thin Solid Films,* **522**, pp. 390–394 (2012).

REFERENCES

[1] *B. Alfano, T. Polichetti, M. Mauriello, M. L. Miglietta, F. Ricciardella, E. Massera, G. Di Francia:* Modulating the sensing properties of graphene through an eco-friendly metal-decoration process (submitted to Sensors and Actuators B).

[2] *M. A. Nigro, G. Faggio, T. Polichetti, F. Ricciardella, F. Fedi, M. L. Miglietta, E. Massera, G. Di Francia: Cross interference effects between water and NH_3 on a sensor based on graphene/silicon Schottky diode.* IEEE Xplore, *AISEM 2015, Feb 3-5, Trento (IT)* (submitted).

[3] *F. Fedi, M. L. Miglietta, T. Polichetti, F. Ricciardella, E. Massera, D. Ninno, G. Di Francia*: Material Research Express **2,** 035601 (2015). (A study on the physicochemical properties of hydroalcoholic solutions to improve the direct exfoliation of natural graphite down to few-layers graphene)

[4] *F. Ricciardella, E. Massera, T. Polichetti, M. L. Miglietta, G. Di Francia:* Applied Physics Letters **104,** 183502 (2014). (A calibrated graphene-based chemi-sensor for sub-ppm NO_2 detection operating at room temperature)

[5] *Y. Grachova, S. Vollebregt, A. L. Lacaita, P. M. Sarro:* Procedia Engineering **87,** 1501 (2014). (High quality wafer-scale CVD graphene on molybdenum thin film for sensing application)

[6] *J. Kumar, Md. Shahabuddin, A. Singh, S. P. Singh, P. Saini, S. K. Dhawan, V Gupta:* Science of Advanced Materials **6,** 1 (2014). (Highly Sensitive Chemo-Resistive Ammonia Sensor Based on Dodecyl Benzene Sulfonic Acid Doped Polyaniline Thin Film)

[7] *Md. Shahabuddina, A. Sharmaa, J. Kumarb, M. Tomarc, A. Umard, V. Gupta:* Sensors and Actuators B **194,** 410 (2014). (Metal clusters activated SnO2 thin film for low level detection of NH3 gas).

[8] *E. Massera, M. L. Miglietta, T. Polichetti, F. Ricciardella, G. Di Francia* in Proceedings of Sensors and Microsystems: AISEM 2013, Feb 5-7, Brescia (IT), 121-125 (2013), Springer International Publishing. (Reproducibility of the performances of graphene based gas sensitive chemiresistors)

[9] *S. Ji, H. Wang, T. Wang, D. Yan:* Advanced Materials **25**, 1755 (2013). (A High-Performance Room-Temperature NO_2 Sensor Based on An Ultrathin Heterojunction Film)

[10] *W. Yuan and G. Shi:* Journal of Materials Chemistry A **1,** 10078 (2013). (Graphene-based gas sensors)

[11] *T. Kobayashi, M. Bando, N. Kimura, K. Shimizu, K. Kadono, N. Umezu, K. Miyahara, S. Hayazaki, S. Nagai, Y. Mizuguchi, Y. Murakami, D. Hobara:* Applied Physics Letters **102,** 023112 (2013). (Production of a 100-m-long high-quality graphene transparent conductive film by roll-to-roll chemical vapor deposition and transfer process)

[12] *J. Wang, B. Singh, S. Maeng, H.-I. Joh, G.-H. Kim:* Applied Physics Letters **103,** 083112 (2013). (Assembly of thermally reduced graphene oxide nanostructures by alternating current dielectrophoresis as hydrogen-gas sensors)

[13] *G. Yang, C. Lee, J. Kim, F. Ren and S. J. Pearton:* Physical Chemistry Chemical Physics **15,** 1798 (2013). (Flexible graphene-based chemical sensors on paper substrates)

[14] E. *Llobet:* Sensors and Actuators B **179,** 32 (2013). (Gas sensors using carbon nanomaterials: A review)

[15] *J. Y. Choi:* Nature Nanotechnology **8**, 311 (2013). (A stamp for all substrates)

[16] *J. Song, F. Y. Kam, R. Q. Png, W. L. Seah, J. M. Zhuo, G. K. Lim, P. K. H. Ho, L. L. Chua:* Nature Nanotechnology **8**, 356 (2013). (A general method for transferring graphene onto soft surfaces)

[17] G. *D. Khuspe, R. D. Sakhare, S. T. Navale, M. A. Chougule, Y. D. Kolekar, R. N. Mulik, R. C. Pawar, C. S. Lee, V. B. Patil:* Ceramics International **39**, 8673 (2013). (Nanostructured SnO2 thin films for NO2 gas sensing applications)

[18] *S. P. Tan and M. Piri:* Industrial and Engineering Chemical Research **52**, 16032 (2013). (Modeling the Solubility of Nitrogen Dioxide in Water Using Perturbed-Chain Statistical Associating Fluid Theory)

[19] *Y. An, A. Behnam, E. Pop, A. Ural:* Applied Physics Letters **102,** 013110 (2013). (Metal-semiconductor-metal photodetectors based on graphene/p-type silicon Schottky junctions)

[20] *A. C. Ferrari and D. M. Basko:* Nature nanotechnology **8,** 235 (2013). (Raman spectroscopy as a versatile tool for studying the properties of graphene)

[21] *F. Torrisi, T. Hasan, W. Wu, Z. Sun, A. Lombardo, T. S. Kulmala, G.-W. Hsieh, S. Jung, F. Bonaccorso, P. J. Paul, D. Chu, A. C. Ferrari:* ACS Nano **6,** 2992 (2012). (Inkjet-Printed Graphene Electronics)

[22] *A. Y. Serov, Z.-Y. Ong, E. Pop:* Applied Physics Letters **102,** 033104 (2013). (Effect of Grain Boundaries on Thermal Transport in Graphene)

[23] *T. Skaltsas, N. Karousis, H.-J. Yan, C.-R. Wang, S. Pispas, N. Tagmatarchis:* Journal of Materials Chemistry **22,** 21507 (2012). (Graphene exfoliation in organic solvents and switching solubility in aqueous media with the aid of amphiphilic block copolymers)

[24] *F. Yavari, E. Castillo, H. Gullapalli, P. M. Ajayan, N. Koratkar:* Appl. Phys. Lett. **100,** 203120 (2012). (High sensitivity detection of NO_2 and NH_3 in air using chemical vapor deposition grown graphene)

[25] *G. Chen, T. M. Paronyan, A. R. Harutyunyan:* Applied Physics Letters **101,** 053119 (2012). (Sub-ppt gas detection with pristine graphene)

[26] *A. W. Robertson, C. S. Allen, Y. A. Wu, K. He, J. Olivier, J. Neethling, A. I. Kirkland, J. H. Warner:* Nature Communications **3,** 1 (2012). (Spatial control of defect creation in graphene at the nanoscale)

[27] *A. Salehi-Khojin, D. Estrada, K. Y. Lin, M.-H. Bae, F. Xiong, E. Pop, R. I. Masel:* Advanced Materials **24,** 53 (2012). (Polycrystalline Graphene Ribbons as Chemiresistors)

[28] *A. Eckmann, A. Felten, A. Mishchenko, L. Britnell, R. Krupke, K. S. Novoselov, C. Casiraghi: Nano Letters* **12,** 3925 (2012). (Probing the Nature of Defects in Graphene by Raman Spectroscopy)

[29] *K. S. Novoselov, V. I. Fal'ko, L. Colombo, P. R. Gellert, M. G. Schwab, K.Kim:* Nature **490**, 192 (2012). (A roadmap for graphene)

[30] *T. Skaltsas, N. Karousis, H. J. Yan, C. R. Wang, S. Pispas, N. Tagmatarchis:* Journal of Material Chemistry **22,** 21507 (2012). (Graphene exfoliation in organic solvents and switching solubility in aqueous media with the aid of amphiphilic block copolymers)

[31] European Environment Agency: *Air quality in Europe — 2012 report,* ISBN 978-92-9213-328-3, ISSN 1725-9177, doi:10.2800/55823.

[32] F. Bonaccorso, A. Lombardo, T. Hasan, Z. Sun, L. Colombo, A. C. Ferrari: *Materials today* ***12,*** 564 (2012). (Production and processing of graphene and 2d crystals)

[33] *Q. H. Wang, K. Kalantar-Zadeh, A. Kis, J. N. Coleman, M. S. Strano:* Nature nanotechnology **7,** 699 (2012). (Electronics and optoelectronics of two-dimensional transition metal dichalcogenides)

[34] *J. N. Coleman:* Accounts of Chemical Research **46,** 14 (2012). (Liquid Exfoliation of Defect-Free Graphene)

[35] *L. G. Cancado, A. Jorio, E. H. Martins Ferreira, F. Stavale, C. A. Achete, R. B. Capaz, M. V. O. Moutinho, A. Lombardo, T. S. Kulmala, A. C. Ferrari:* Nano Letters **11,** 3190 (2011). (Quantifying Defects in Graphene via Raman Spectroscopy at Different excitation energies)

[36] *G. Lu, S. Park, K. Yu, R. S. Ruoff, L. E. Ocola, D. Rosenmann, J. Chen:* ACS Nano **5,** 1154 (2011). (Toward Practical Gas Sensing with Highly Reduced Graphene Oxide: A New Signal Processing Method To Circumvent Run-to-Run and Device-to-Device Variations)

[37] *F. Ricciardella:* Master thesis, Università degli Studi di Bari "A. Moro" (2011).

[38] *F. Ricciardella, I. Nasti, T. Polichetti, M. L. Miglietta, E. Massera, S. Romano, G. Di Francia* in Selected papers from the Workshop on Fundamentals and Applications of Graphene; L. Ottaviano e V. Morandi (Editors), **ISBN 978-3-642-20643-6.** (2011)

[39] *S. Dhar, A. Roy Barman, G. X. Ni, X. Wang, X. F. Xu, Y. Zheng, S. Tripathy, Ariando, A. Rusydi, K. P. Loh, M. Rubhausen, A. H. Castro Neto, B. O˝ zyilmaz, T. Venkatesan:* AIP ADVANCES **1,** 022109 (2011). (A new route to graphene layers by selective laser ablation)

[40] *M. Qian, Y. S. Zhou, Y. Gao, J. B. Park, T. Feng, S. M. Huang, Z. Sun, L. Jiang, Y. F. Lu:* Applied Physics Letters **98,** 173108 (2011). (Formation of graphene sheets through laser exfoliation of highly ordered pyrolytic graphite)

[41] Office of Air and Radiation (6301A) EPA-456/F-11-003: *Air quality guide for NO_2 (2011).*

[42] *C.C. Chen, M. Aykol, C.C. Chang, A.F.J. Levi, S.B. Cronin:* Nano Letters **11**, 1863 (2011). (Graphene-Silicon Schottky Diodes)

[43] *W. Regan, N. Alem, B. Alemán, B. Geng, Ç. Girit, L. Maserati, F. Wang, M. Crommie, A. Zettl:* Applied Physics Letters **96**, 113102 (2010). (A direct transfer of layer-area graphene)

[44] *U. Khan, A. O'Neill, M. Lotya, S. De, J. N. Coleman:* Small **6,** 864 (2010). (High-Concentration Solvent Exfoliation of Graphene)

[45] *S. Bae, H. Kim, Y. Lee, X. Xu, J.-S. Park, Y. Zheng, J. Balakrishnan, T. Lei, H. R. Kim, Y. I. Song, Y.-J. Kim, K. S. Kim, B. O¨zyilmaz, J.-H. Ahn, B. H. Hong, S. Iijima:* Nature Nanotechnology **5,** 574 (2010). (Roll-to-roll production of 30-inch graphene films for transparent electrodes)

[46] *F. Banhart, J. Kotakoski, A. V. Krasheninnikov:* ACS Nano **5,** 26 (2010). (Structural Defects in Graphene)

[47] *H. J. Park, J. Meyer, S. Roth, V. Skákalová:* Carbon **48,** 1088 (2010). (Growth and properties of few-layer graphene prepared by chemical vapor deposition)

[48] *J. H. Seol, I. Jo, A. L. Moore, L. Lindsay, Z. H. Aitken, M. T. Pettes, X. Li, Z. Yao, R. Huang, D. Broido, N. Mingo, R. S. Ruoff, L. Shi:* Science **328**, 213 (2010). (Two-Dimensional Phonon Transport in Supported Graphene)

[49] *M. Kalbac, A. Reina-Cecco, H. Farhat, J. Kong, L. Kavan, M. S. Dresselhaus: ACS Nano **4**, 6055* (2010). (The Influence o**f** Strong Electron and Hole Doping on the Raman Intensity of C*hemical Vapor-Deposition Graphene)*

[50] *F. Bonaccorso, Z. Sun, T. Hasan, A. C. Ferrari:* Na**t**ure Photonics **4,** 611 (2010). (Graphene photonics and optoelectronics)

[51] *C. Soldano, A. Mahmood, E. Dujardin:* Carbon **48,** 2127 (2010). (Production, properties and potential of graphene)

[52] *A. Balan, R. Kumar, M. Boukhicha, O. Beyssac, J.-C. Bouillard, D. Taverna, W. Sacks, M. Marangolo, E. Lacaze, R. Gohler, W. Escoffier, J.-M. Poumirol, A. Shukla:* Journal Of Physics D: Applied Physics **43**, 374013 (2010). (Anodic bonded graphene)

[53] *A. K. Geim:* Science **324,** 1530 (2009). (Graphene: Status and Prospects)

[54] *Y.-H. Zhang, Y.- B. Chen, K.- G. Zhou, C.- H. Liu, J. Zeng, H.- L. Zhang, Y. Peng:* Nanotechnology **20**, 185504 (2009). (Improving gas sensing properties of graphene by introducing dopants and defects: a first-principles study)

[55] *G. Cantele, Y.-S. Lee, D. Ninno, N. Marzari:* Nano Letters **9,** 3425 (2009). (Spin Channels in Functionalized Graphene Nanoribbons)

[56] *K. V. Emtsev, A. Bostwick, K. Horn, J. Jobst, G. L. Kellogg, L. Ley, J. L. McChesney, T. Ohta, S. A. Reshanov, J. Röhrl, E. Rotenberg, A. K. Schmid, D. Waldmann, H. B.Weber, T. Seyller:* Nature materials **8**, 203 (2009) (Towards wafer-size graphene layers by atmospheric pressure graphitization of silicon carbide)

[57] *A. Shukla, R. Kumar, J. Mazher, A. Balan:* Solid State Communications **149**, 718 (2009). (Graphene made easy: High quality, large-area samples)

[58] *K. S. Kim, Y. Zhao, H. Jang, S. Y. Lee, J. M. Kim, K. S. Kim, J.-H. Ahn, P. Kim, J.-Y. Choi, B. H. Hong:* Nature **457,** 706 (2009). (Large-scale pattern growth of graphene films for stretchable transparent electrodes)

[59] *A. B. Kuzmenko, E. van Heumen, F. Carbone, D. van der Marel:* Physical Review Letters **100**, 117401 (2008). (Universal Optical Conductance of Graphite)

[60] *R. R. Nair, P. Blake, A. N. Grigorenko, K. S. Novoselov, T. J. Booth, T. Stauber, N. M. R. Peres, A. K. Geim:* Science **320,** 1308 (2008). (Fine Structure Constant Defines Visual Transparency of Graphene)

[61] *C. Lee, X. Wei, J. W. Kysar, J. Hone:* Science **321**, 385 (2008). (Measurement of the Elastic Properties and Intrinsic Strength of Monolayer Graphene)

[62] *A. A. Balandin, S. Ghosh, W. Bao, I. Calizo, D. Teweldebrhan, F. Miao, C. N. Lau:* Nano Letters **8,** 902 (2008). (Superior Thermal Conductivity of Single-Layer Graphene)

[63] *D. W. Boukhvalov, M. I. Katsnelson:* Nano Letters **8,** 4373 (2008). (Chemical functionalization of graphene with defects)

[64] *J. T. Robinson, F. K. Perkins, E. S. Snow, Z. Wei, P. E. Sheehan:* Nano Letters **8,** 3137 (2008). (Reduced Graphene Oxide Molecular sensors)

[65] *S. V. Morozov, K. S. Novoselov, M. I. Katsnelson, F. Schedin, D. C. Elias, J. A. Jaszczak, A. K. Geim:* Physics Review Letter **1,** 016602 (2008). (Giant intrinsic carrier mobilities in graphene and its bilayer)

[66] *K. I. Bolotin, K.J. Sikesb, Z. Jianga,d, M. Klimac, G. Fudenberga, J. Honec, P. Kima, H.L. Stormer:* Solid State Communications **146,** 351 (2008). (Ultrahigh electron mobility in suspended graphene)

[67] *X. Du, I. Skachko, A. Barker, E. Y. Andrei:* Nature nanotechnology **3,** 491 (2008). (Approaching ballistic transport in suspended graphene)

[68] *Y. Hernandez, V. Nicolosi, M. Lotya, F. M. Blighe, Z. Sun,S. De, I. T. Mcgovern, B. Holland, M. Byrne, Y. K. Gun'ko, J. J. Boland, P. Niraj, G. Duesberg, S. Krishnamurthy, R. Goodhue, J. Hutchison, V. Scardaci, A. C. Ferrari, J. N. Coleman:* Nature nanotechnology **3**, 563 (2008). (High-yield production of graphene by liquid-phase exfoliation of graphite)

[69] *A. K. Geim and K. S. Novoselov:* Nature **6,** 169 (2007). (Graphene calling)

[70] *A. K. Geim and K. S. Novoselov:* Nature **6,** 183 (2007). (The rise of graphene)

[71] *F. Schedin, A. K. Geim, S. V. Morozov, E. W. Hill, P. Blake, M. I. Katsnelson, K. S. Novoselov: Nature **6,** 652* (2007). (Detection of individual gas molecules adsorbed on graphene)

[72] *E. Cappelli, S. Orlando, V. Morandi, M. Servidori, C. Scilletta:* Journal of Physics: Conference Series **59**, 616 (2007). (Nano-graphene growth and texturing by Nd:YAG pulsed laser ablation of graphite on Silicon)

[73] *A.C. Ferrari:* Solid State Communications **143,** 47 (2007). (Raman spectroscopy of graphene and graphite: Disorder, electron–phonon coupling, doping and nonadiabatic effects)

[74] *H. C. Schniepp, J.-L. Li, M. J. McAllister, H. Sai, M. Herrera-Alonso, D. H. Adamson, R. K. Prud'homme, R. Car, D. A. Saville, I. A. Aksay:* Journal of Physical Chemistry B **110,** 8535 (2006). (Functionalized single graphene sheets derived from splitting graphite oxide)

[75] *S. Stankovich, D. A. Dikin, G. H. B. Dommett, K. M. Kohlhaas, E. J. Zimney, E. A. Stach, R. D. Piner, S. T. Nguyen, R. S. Ruoff:* Nature **442**, 282 (2006). (Graphene-Based Composite Materials)

[76] *A. C. Ferrari, J. C. Meyer, V. Scardaci, C. Casiraghi, M. Lazzeri, F. Mauri, S. Piscanec, D. Jiang, K. S. Novoselov, S. Roth, A. K. Geim: Physical Rewiev Letters* **97**, 187401 (2006). (Raman Spectrum of Graphene and Graphene Layers)

[77] *E. Rollings, G.H. Gweona, S.Y. Zhoua, B.S. Munb, J.L. McChesneyc, B.S. Hussainb, A.V. Fedorovc, P.N. Firstd, W.A. de Heerd, A. Lanzara:* Journal of Physics and Chemistry of Solids **67**, 2172 (2006). (Synthesis and characterization of atomically thin graphite films on a silicon carbide substrate)

[78] *S. T. Shishiyanu, T. S. Shishiyanu, O. I. Lupan;* Sensors and Actuators B **107**, 379 (2005). (Sensing characteristics of tin-doped ZnO thin films as NO_2 gas sensor)

[79] *K. S. Novoselov, D. Jiang, F. Schedin, T. J. Booth, V. V. Khotkevich, S. V. Morozov, A. K. Geim:* Proceedings of the National Academy of Sciences USA **102,** 10451 (2005). (Two-dimensional atomic crystals)

[80] *K. S. Novoselov, A. K. Geim, S. V. Morozov, D. Jiang, M. I. Katsnelson, I. V. Grigorieva, S. V. Dubonos, A. A. Firsov:* Nature **438,** 197 (2005). (Two-dimensional gas of massless Dirac fermions in graphene)

[81] *V. P. Gusynin and S. G. Sharapov:* Physical Review Letters **95**, 146801 (2005). (Unconventional Integer Quantum Hall Effect in Graphene)

[82] *K. S. Novoselov A. K. Geim, S. V. Morozov,2 D. Jiang, Y. Zhang, S. V. Dubonos, I. V. Grigorieva, A. A. Firsov:* Science **306**, 666 (2004). (Electric Field Effect in Atomically Thin Carbon Films)

[83] DIRECTIVE 2008/50/EC

[84] DIRECTIVE 2001/81/EC

[85] *A. C. Ferrari and J. Robertson:* Physical Review B **61,** 14095 (2000). (Interpretation of raman spectra of disordered and amorphous carbon)

[86] *S. Capone, A. Forleo, L. Francioso, R. Rella, P. Siciliano, J. Spadavecchia, D. S. Presicce, A. M. Taurino:* Solid State Gas Sensors: State Of The Art And Future Activities. Journal of Optoelectronics and Advanced Materials **5,** 1335 (2003).

[87] *S. Hahn,* Ph.D. Thesis, Universität Tübingen (2002).

[88] Occupational Safety and Health guideline for Ammonia (U.S. Department of Health and Human Services, 1992)

[89] *S. Sze:* Physics of Semiconductor Devices. Wiley-Interscience publication. John Wiley & Sons, 1981.

[90] *W. S. Hummers, R. E. Offeman:* Journal of American Chemistry Society **80,** 1339 (1958). (Preparation of graphite oxide)

[91] http://www2.worksafebc.com

[92] *T. Moldt, A. Eckmann, P Klar, S. V. Morozov, A. A. Zhukov, K. S. Novoselov, C. Casiraghi:* ACS Nano **5,** 7700 (2011). (High-Yield Production and Transfer of Graphene Flakes Obtained by Anodic Bonding)

[93] *G. Lu, L. E. Ocola, J. Chen:* Nanotechnology **20,** 445502 (2009). (Reduced graphene oxide for room-temperature gas sensors)

[94] *M. A. Pimenta, G. Dresselhaus, M. S. Dresselhaus, L. G. Cancado, A. Jorio, R. Saito:* Physical Chemistry Chemical Physics **9**, 1276 (2007). (Studying disorder in graphite-based systems by Raman spectroscopy)

[95] *A. Pirkle, J. Chan, A. Venugopal, D. Hinojos, C. W. Magnuson, S. McDonnell, L. Colombo, E. M. Vogel, R. S. Ruoff, R. M. Wallace:* Applied Physics Letters **99,** 122108 (2011). (The effect of chemical residues on the physical and electrical properties of chemical vapor deposited graphene transferred to SiO2)

[96] *F. Ricciardella, B. Alfano, F. Loffredo, F. Villani, T. Polichetti, M. L. Miglietta, E. Massera, G. Di Francia:* Inkjet printed graphene-based chemi-resistors for gas detection in environmental conditions. IEEE Xplore, *AISEM 2015, Feb 3-5, Trento (IT)* (submitted)

[97] *F. Fedi, F. Ricciardella, M. L. Miglietta, T. Polichetti, E. Massera and G. Di Francia:* Easy recovery method for graphene-based chemi-resistors, *A. D'Amico et al. (eds.), Sensors and Microsystems: AISEM 2014 Proceedings, Lecture Notes in Electrical Engineering **109,** 121, Springer Science + Business Media, LLC 2014.*

[98] *F. Fedi, F. Ricciardella, M. L. Miglietta, T. Polichetti, E. Massera, G. Di Francia:* Journal of Sensors and Sensor Systems **3,** *241 (2014). (*A simple method to recover the graphene-based chemi-resistors signal)

[99] *S. Cui, S. Mao, Z. Wen, J. Chang, Y. Zhang, J. Chen:* Analyst **138,** 2877 (2013). (Controllable synthesis of silver nanoparticle-decorated reduced graphene oxide hybrids for ammonia detection)

[100] *Q. T. Tran, H. T. M. Hoa, D. H. Yoo, T. V. Cuong, S. H. Hur, J. S. Chung, E. J. Kim, P. A. Kohl:* Sensors and Actuators B **194,** 45 (2014). (Reduced graphene oxide as an over-coating layer on silver nanostructures for detecting NH_3 gas at room temperature)

[101] *A. Kaniyoor, R. I. Jafri, T. Arockiadoss. S. Ramaprabhu:* Nanoscale **1,** 382 (2009). (Nanostructured Pt decorated graphene and multi walled carbon nanotube based room temperature hydrogen gas sensor)

[102] *M. Gautam and A. H. Jayatissa:* Solid-State Electronics **78,** 159 (2012). (Ammonia gas sensing behaviour of graphene surface decorated with gold nanoparticles)

[103] *B. H. Chu, C. F. Lo, J. Nicolosi, C. Y. Chang, V. Chen, W. Strupinski, S. J. Pearton, F. Ren:* Sensor and Actuators B **157,** 500 (2011). (Hydrogen detection using platinum coated graphene grown on SiC)

ACKNOWLEDGEMENTS

Since the Bachelor's degree to conclude with the PhD, I had the pleasure and the honor to attend any sitting of degree and I witnessed a strange phenomenon in consultation with the thesis: the frenzied run-up to the final part of the thesis that encloses the thanks and the spasmodic search for your own name in the list of people reported there. Beyond the various more or less shared interpretations, what is certain is that thanks have a significant weight in the economy of work, especially for the author and, why not, even for readers. The risk of making wrong to someone is lurking, however trying to resume three years, or more, of your own life in just a few lines is quite impractical. By the way, let me try.

The first big thank can only be addressed to the person who has permitted and made sure I started and ended up the PhD, my tutor Tiziana. The not wanting to achieve a PhD was one of my more assertive certainty since the beginning of the academic career and instead ... instead she, graciously and quietly, as her costume, managed to insinuate doubt at the end of my master degree. Considered my renamed stubbornness, she has the merit to be successful in the work of conviction which costs me quite a few dinners with friends and relatives to be fallen into contradiction. I never considered the Tutor – I have and continuously call her in this way so many times to fear that sometimes she was extremely angry with me – as my boss, as people usual wonders around the world, but for me she was and will always be the person who started my scientific career. In addition to countless scientific teachings, I am grateful to her for the way almost maternal to treat a person by the character strong enough like me: in almost five years, some diplomatic accident was lightly touched. But the almost total uniformity of views has made negligible the few unavoidable accidents, due mainly to my obsessive and manic desire to arrange the detail and its manner of proceeding step by step. As the Roman miser stated in the satire of Horace, "when the people submerged me of whistles, she has been one of the few people to believe in the coins contained in the chest". For this and for bringing me at this point I will be grateful to her…forever.

A great deal of thanks goes to the other members of my workgroup: Mara, Ettore, Filippo and Girolamo. To all of them, I want to express my special thank:

- Mara has become one of my greatest confident and, in spite of during my master degree she was very severe with me, during the PhD time I have appreciated lot her sincerity with me;

- Ettore has teached to me almost all I know in the gas sensors field. I asked to him so many questions and explanations that I renamed him “maestro”;

- Filippo, who was the first master student which I collaborate with during my PhD, has become one of the most nice friends. Thanks for the fruitful brain-storming which we had and we are continuously having nevertheless his PhD in Austria;

- last but definitively not least, Girolamo - I always have called him dr. Di Francia and maybe this is the first time I am calling him with his first name – sometimes has been with me stronger than my father but he has continuously given me (and I hope to still receive) notable advices and helpful suggestions not only for my research activity. Thanks to all of you also for teaching me to work in team and, maybe, without your help, I would not be arrived to this point in my knowledge and… in my life.

Thanks are extended to three wonderful guys, Arcangela, Brigida and Riccardo, which I worked with in the last part of my PhD. I particularly remember and appreciate all the valuable discussions and the pleasant interactions with them, not only for scientific purposes but also for their tips. I will always bring with me the Riccardo’s positive message he gave to me in the mail he wrote when we said goodbye.

I would like to express my gratitude to prof. Ninno, my academic tutor: his precise suggestions at the exact time have been of fundamental importance for my PhD. As I said to him, I never tough to find an academic person like him, with his appreciable frankness and sincerity. He has shown to me another side of academic life. Thanks!

I am thankful to my ENEA officemates Libero and Antonio for supporting me the whole way and encouragement: in all hard moments talking and confide in them has helped me to go on and, why not, to arrive at this point.

I would to thank Emilia, Iurie, Fulvia, Fausta, Paola, Tommaso, Peppe Nenna, Peppe Pandolfi, Franco Pascarella, Antonio Citarella, Raffele, Luana, Antonio Agati and all people I call the ENEA family: just only one word from you and your trust in me have been significant.

My deepest gratitude and acknowledgement are expressed to prof. Lina Sarro and especially to Sten Vollebregt. Prof. Sarro was extremely gentle not only in accepting me during the stage at TU Delft but also in all our fruitful discussions. Sten, my daily supervisor or, as I called him "daily teacher", during the period at TU Delft, introduced me in the activity concerning graphene so clearly that I acquired very rapidly a great experience in the world of the CVD technique. I would like to express my special thanks to Sten, firstly, to believe in my wok, then for the brain-storming discussions in which experiences were shared and great ideas were generated. I really enjoyed my time there and I deeply hope to share again work with him in future.

Thanks to Giuseppe Fiorentino, Nikolas Gaio and Nello Franzese for the welcome in TU Delft when I arrived and for the first help for the initial arrangement and fruitful discussions.

I wish to thank Giuseppe Colucci and Limor for their kind and funny company during my time in Delft.

Special thank goes to my Portici housemates Fiorenzo, Gianni, Pierpaolo and Roberto: their pleasant company, our hobbies in the evenings (puzzles, burraco matches, football, TV) and our dinners together have made more amusing the PhD time.

Special thanks to two really special persons, my friends Enzo and Paola: their kind friendship and their availability in helping me for whatever and whenever will be one of the best memories of my PhD time. With them I thank all my friends who have supported me in all my choices.

At the end, going a while back in the last three years, I would like also to thank those people who, intentionally or unintentionally, in and out the workplace, have made more tortuous my way… despite of them, the finishing line has been reached. Thanks to all of you and…ad maiora semper!

The final and most important acknowledgement go to my parents, Filomena and Savino, who once more have supported me in all the situations and never did miss their priceless tips, to my sister Rosanna, my brother-in-law Vito and my delicious little niece Emanuela, who has made glad some sad days.